

UCSF

UC San Francisco Electronic Theses and Dissertations

Title

Signaling Interactions that Control Bone Formation in the Lower Jaw

Permalink

<https://escholarship.org/uc/item/5sx5x1vp>

Author

Nguyen, An Nhat Duy

Publication Date

2023

Peer reviewed|Thesis/dissertation

Signaling Interactions that Control Bone Formation in the Lower Jaw

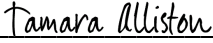
by
An Nhat Duy Nguyen

DISSERTATION
Submitted in partial satisfaction of the requirements for degree of
DOCTOR OF PHILOSOPHY

in
Oral and Craniofacial Sciences

in the
GRADUATE DIVISION
of the
UNIVERSITY OF CALIFORNIA, SAN FRANCISCO

Approved:


DocuSigned by:

E233CABEF261499... Tamara Alliston
Chair

DocuSigned by:

Ralph Marcucio

DocuSigned by:

Licia Selleri

DocuSigned by:

C704CE82E8E34CE... Richard A. Schneider

Committee Members

Copyright 2023

by

An Nhat Duy Nguyen

Dedication

To my parents and Daniel, who have been my endless source of support.

~~~

In memory of my beloved cousin, Lily Pham, who taught me to live life to the fullest and to never give up on my dream.

~~~

Acknowledgements

The work conducted in Chapter 1 was initiated by Dr. Jennifer Fish and Dr. Zuzka Vavrušová, who generated chimeric animals and processed the tissues.

For the work conducted in Chapter 2, I thank A. Barczak and J. Pollack at the Sandler Center Functional Genomics Core for the preliminary RNA-seq analysis, and A. Hardin and N. Ahituv for help with the in-depth RNA-seq analysis.

For the work conducted in Chapter 3, Dr. Daniel Chu engineered the overexpressing system and performed all the molecular modifications to the plasmid backbones.

I would like to thank my lab members for creating a supportive and friendly lab environment where help has been always available and failed experiments have always turned into valuable lessons for the next steps through our deep discussions and weekly three-to-four-hour long lab meetings. I am forever thankful for Dr. Rich A. Schneider for his willingness to go above and beyond in supporting his trainees, and for always making himself available to help me with numerous rounds of revisions for writing grants,

applications, papers, and my dissertation. I am grateful for Dr. Daniel Chu's expertise and his generosity with his time in helping me troubleshoot experiments. I thank Dr. Zuzka Vavrušová for her constant moral support and helpful advice, as well as Dr. Spenser Smith for being a supportive lab member. For members from other labs, I thank Dr. Stefan Dudli from the Fields Lab and Dr. Neha Dole from the Alliston Lab who helped me with data analysis on qPCR, and Dr. Mohamed Habib from Fields Lab who helped me with processing samples for μ CT scanning.

I am thankful for the supportive Oral Craniofacial Sciences Graduate Program, especially my Graduate Advisor, Dr. Pamela Den Besten, for her advice and support, and the Program Coordinator, Roger Mraz, for always pointing me in the right direction.

Special thanks to my committee, including Dr. Tamara Alliston, Dr. Ralph Marcucio, Dr. Licia Selleri, and especially my advisor, Dr. Rich A. Schneider, for their constructive feedback, their helpful ideas on experiments to perform, and their kind guidance on my academic training and career.

I would like to thank the following sources of funding: NIDCR F30 Award (F30 DE027616), Discovery Fellowship, AADR Fellowship, Osher Scholarship, Maxwell Scholarship, Graduate Division Travel Award, AADR Bloc Travel Grant, Henry Thornton SCADA Scholarship, and Dental Alumni Association Humanitarian Award.

Nothing in life is to be feared; it is only to be understood.

-Marie Curie

Abstract

Signaling Interactions that Control Bone Formation in the Lower Jaw

An Nhat Duy Nguyen

Identifying molecular signals mediating the epithelial-mesenchymal interactions (EMI) required for bone formation in the embryonic jaw skeleton could lead to the discovery of novel proteins with therapeutic potential for regenerating bone in cases of disease and injury. An RNA-seq strategy was used to identify candidate genes involved in the EMI of the mandibular primordia, which give rise to the lower jaw.

RNA in situ hybridization and RT-qPCR were used to characterize the spatiotemporal expression of these genes qualitatively and quantitatively on the mRNA levels in three avian species (duck, quail, and chicken). In vitro organ cultures were used to test if the expression of these genes in mandibular mesenchyme requires epithelial signaling. Gain- and loss-of-function experiments tested if these genes regulate mandibular osteogenesis. Results from the RNA-seq experiment, RNA in situ, and RT-qPCR reveal that spatiotemporal changes in members of the CXC and WNT signaling pathways are present at the right time, place, and levels to mediate the osteogenic EMI in the mandibular primordia. In vitro organ cultures confirmed that mesenchymal expression of these genes depends on epithelial signaling. Gain-of-function experiments revealed that CXCL14 is sufficient to augment bone formation compared to the non-treated side after seven days of culture. Loss-of-function experiments demonstrated that WNT signaling is required for mandibular osteogenesis but that CXCL14 can restore bone formation in the absence of WNT signaling. Moreover, altering the WNT pathway affects CXCL14 expression, suggesting that CXCL14 acts downstream of WNT ligands.

Table of Contents

Chapter 1: Introduction	1
Chapter 2: An Experimental Strategy Using RNA-seq To Identify Differentially Expressed Epithelial Genes During Mandibular Osteogenesis	13
Chapter 3: An Experimental Strategy For Mis-Expressing Genes-of-Interest Using Stable Integration of An Inducible Promoter System	28
Chapter 4: A Role for CXCL14 and WNT Signaling in Mediating the Epithelial- Mesenchymal Interactions Required for Mandibular Osteogenesis	42
Chapter 5: Summary and Future Directions	83
References	89

List of Figures

Figure 2.1: RNA seq experiment and RT-qPCR experiment to identify and validate expression of candidate genes.	22
Figure 2.2: An overview of read coverage and mapped reads of the RNA-seq dataset.	23
Figure 2.3: Venn diagram of differentially expressed genes.	24
Figure 2.4: Pathway analysis for differentially expressed genes.	25
Figure 2.5: Log2 fold change graph for differentially expressed genes.	26
Figure 2.6: List of identified candidate genes that are secreted molecules.	27
Figure 3.1: Time course imaging of HH21 chick mandibular primordia overexpressing <i>Cxcl14</i>	39
Figure 3.2: Validation of successful overexpression of pEPIC1.1- <i>Cxcl14</i>	40
Figure 3.3: Validation of successful overexpression of pPIDNB- <i>Cxcl14</i>	41
Figure 4.1: CXCL14 protein sequence overview.	68
Figure 4.2: Heat map analysis of genes differentially expressed in Duck HH24 vs Duck HH27 and Duck HH24 vs Quack HH24.	69
Figure 4.3: <i>Cxcl14</i> and <i>Wnt11</i> expression in Chick mandibular primordia.	70
Figure 4.4: <i>Cxcl14</i> overexpression and early mesenchymal condensation.	71
Figure 4.5: <i>Cxcl14</i> overexpression and early bone formation.	72
Figure 4.6: Quantification of bone formation in mandibles overexpressing <i>Cxcl14</i> vs controls.	73

Figure 4.7: In vivo induction of <i>Cxcl14</i> in chick mandibular primordia.	74
Figure 4.8: Verification of overexpression level of <i>Cxcl14</i>	75
Figure 4.9: The role of <i>Cxcl14</i> in regulating bone formation.	76
Figure 4.10: The role of <i>Cxcl14</i> in regulating bone formation.	77
Figure 4.11: Quantification of bone formation in <i>Cxcl14</i> OE sides vs control sides.	78
Figure 4.12: Altering WNT signaling and the resulting phenotypes.	79
Figure 4.13: Quantification of bone formation resulting from activating and inhibiting WNT signaling.	80
Figure 4.14: WNT signaling as an upstream regulator of <i>Cxcl14</i>	81
Figure 4.15: Abnormally longer lower jaw found in quail overexpressing <i>Cxcl14</i>	82
Figure 5.1: <i>Cxcl14</i> loss-of-function experiment using RCAS-shRNA.	88

Chapter 1: Introduction

Clinical Significance

Craniofacial anomalies are among the most common birth defects (Gorlin et al., 1990; Parker et al., 2010). Many of these arise from perturbations to the embryonic formation of bone (Schneider, 2015). For example, malformations such as cleft palate and jaw length defects can be caused by disruptions to the rate of proliferation or timing of differentiation of neural crest mesenchyme (NCM), which are the skeletal progenitor cells in the face and jaws (Ito et al., 2003; Oka et al., 2007; Satokata and Maas, 1994; Sharpe and Ferguson, 1988; Van Exan and Hall, 1984). In syndromes such as Treacher Collins, the generation, migration, and differentiation of NCM are compromised in ways that cause mandibular hypoplasia and other debilitating conditions (Dixon et al., 2006; Jones et al., 2008; Trainor et al., 2009). Babies born with a small lower jaw skeleton often face immediate life-threatening problems like airway obstruction, aspiration, difficulty feeding, and failure to thrive. To repair such devastating congenital anomalies, surgeons typically perform extensive and repeated surgeries on the skeleton that are costly, painful, and compromise the quality of life for patients (Jenzer and Schlam, 2022). Similar types of surgeries are also employed for skeletal defects that result from trauma, neoplasm, and other diseases. One of the biggest challenges in these types of surgeries is having enough osseous material to augment the surgical healing process especially when the patient's own bone is deficient, and so a common strategy that remains the gold standard is the use of bone grafts (Aaboe et al., 1995).

Humans have had a keen interest in bone graft procedures for millennia and some of the earliest archaeological evidence for bone grafts can be seen around 656 – 535 BCE

when ancient Egyptians transplanted a limb from an Ethiopian to a Justinian (Hampel et al., 2022). Job van Meekeren has been credited as the first modern surgeon to perform a heterologous bone graft procedure from a dog skull fragment into an injured soldier's skull in 1668 (de Boer, 1988; Hampel et al., 2022). Interestingly, the patient was later excommunicated by the church because of the unprecedented surgery that was deemed "un-Christian" and thus demanded that the Dutch surgeon remove the graft; however, the dog bone fragment was integrated and became part of the patient's cranium (de Boer, 1988; Hampel et al., 2022). This successful bone graft surgery revealed the potential of transplanting bone, yet these surgeries were uncommon until 1880 when William Macewen performed the first case in which he put a tibia in place of an infected humerus from a four-year-old boy with rickets (de Boer, 1988). However, not all early bone grafts were successful. In 1891, Phelps grafted a piece of dog bone into a defective tibia of a boy, and he kept the donor and host attached for two weeks. The graft subsequently failed in five weeks and had to be removed (de Boer, 1988; Phelps, 1891). From 1915-1920, Hibbs, Albee, and Sheen performed hundreds of successful bone graft cases, including treatments of Pott's disease in patients with tuberculous spine that was replaced with tibial grafts, which marked the new era of bone graft surgery (Hampel et al., 2022).

In orthopaedic as well as oral and maxillofacial surgery, bone graft materials have progressively evolved over time. Clinically, there are many options for bone graft sources, including xenografts (bone taken from a different species, commonly bovine), allografts (bone taken from a different individual of the same species), and autografts (bone taken from the same individual). Bone grafts materials can carry one or multiple properties:

osteoconductive, osteoinductive, and osteogenic (Albrektsson and Johansson, 2001). Materials with osteoconductive properties can enhance the migration of osteoblasts and their progenitor cells. Materials with osteoinductive properties can induce the differentiation of osteoblast lineage. Materials with osteogenic properties can form bone and thus are regarded as the best option in terms of osteogenesis. Autologous bone grafts are considered the most superior strategy as they possess all three properties (osteoconductive, osteoinductive, and osteogenic) yet their biggest disadvantage is their limited availability from donor sites and associated morbidities from the harvesting procedure (Albrektsson and Johansson, 2001).

In the context of the oral cavity, bone defects are often found in congenital skeletal anomalies, periodontal diseases, traumas, and neoplasm. In jaw reconstruction cases, a fibula is often grafted into defects of moderate to large sizes. However, a fibula is too straight to replicate the contour of the facial skeleton like a mandible. Also, the size discrepancy between the graft and the accepted site is critical to consider for autograph approaches. Importantly, during the healing process, a bony callus can form at the junction between the graft and the host bone, which consists of osteoid that directs the integration of the graft. Therefore, signals that induce osteoid formation may potentially function as therapeutic agents for regenerating bone. Notably, pathologic conditions like osteoporosis, radiation-induced-osteonecrosis, and bisphosphonates-induced-osteonecrosis also severely affect the jaws and their associated bone loss could benefit from novel osteogenic therapies. Thus, there has long been an unmet need to find new sources for bone graft materials, and solving this problem, especially by devising novel

molecular- and cell-based strategies to stimulate the formation of de novo bone, has been a goal of many researchers and clinicians.

In terms of molecular-based therapies, Bone Morphogenetic Proteins (BMPs), which were discovered in 1965, are among the first recombinant proteins to be used as bone graft substitutes (Urist, 1965). BMPs belong to the transforming growth factor beta superfamily and are the most extensively studied molecule with applications for treating skeletal defects (Balk et al., 1997; Kloen et al., 2002; Li et al., 2002; Wang et al., 1993). The only two BMPs that are currently FDA approved are recombinant (r) human (h) BMP2 and rhBMP7 (Henderson et al., 2016; Kanakaris et al., 2008). BMPs are osteoinductive, and thus, because they are not considered to be osteoconductive or osteogenic, BMPs are often combined with an osteoconductive carrier such as collagen, allografts, or autografts as a means to improve bone integration and rates of healing (Boden et al., 2002; Kim and Valentini, 2002; Miyamoto and Takaoka, 1993).

However, there remain many concerns about potential adverse side effects of BMPs including inflammation, life-threatening swelling, hematoma, ectopic bone formation, bone resorption mediated by osteoclasts, and tumorigenesis (James et al., 2016). Additionally, there have been doubts regarding the clinical benefits and cost-effectiveness of using BMPs (Garrison et al., 2010). In particular, some meta-analyses have suggested that when BMPs are used in bone fractures, their ability to significantly increase healing rates (95% CI 0.90 to 1.15) is unclear compared to control groups (Garrison et al., 2010). Although BMPs have played a revolutionary role in the field of bone graft substitutes, their

limited and controversial efficacy as well as their many adverse side-effects when treating skeletal defects, beg for more research in finding additional novel osteogenic factors to expand our existing tool kit and enhance bone formation during repair and regeneration. This is the primary goal of my thesis project and my future work. My current strategy to accomplish this goal has been to investigate the signaling interactions among different embryonic tissues that underlie mandibular osteogenesis.

Epithelial-Mesenchymal Interactions During Mandibular Osteogenesis

Jaw bones arise from NCM that migrates out of the dorsal margins of the neural folds into the facial primordia. NCM gives rise to osteoblasts and subsequent bone formation occurs through intramembranous ossification whereby osteoblasts secrete osteoid directly into the extracellular matrix rather than replace a preformed cartilaginous template (Helms and Schneider, 2003). By contrast, bone in the base of the skull, appendicular skeleton such as the limbs, and axial skeleton such as the vertebrae, replaces cartilage via endochondral ossification (Noden and Schneider, 2006). The lower jaw contains a central cartilage element called Meckel's cartilage that serves as a scaffold around which NCM gives rise to bone via intramembranous ossification.

Precisely timed interactions between NCM and mandibular epithelium are required for intramembranous ossification of the lower jaw skeleton (Hall, 2000; Hall and Miyake, 1992; Helms and Schneider, 2003; Merrill et al., 2008). That these interactions are osteo-inductive and stage-dependent has been revealed through tissue recombination and epithelial removal experiments using chick and mouse embryos (Bradamante and Hall,

1980; Dunlop and Hall, 1995; Francis-West et al., 1998; Hall, 1978, 1982; Hall and Coffin-Collins, 1990; Helms and Schneider, 2003; Merrill et al., 2008; Sharpe and Ferguson, 1988; Tyler and Hall, 1977; Tyler and McCobb, 1980; Vaglia and Hall, 1999; Van Exan and Hall, 1984; Wedden, 1987). Previous studies in chicken and the work from our lab in quail and duck have shown that mesenchyme depends on epithelial signals for bone formation during the first few days of development (Hall, 1978; Merrill et al., 2008; Tyler and Hall, 1977).

As in the development of teeth and limb buds, there are reciprocal interactions between mandibular epithelium and mesenchyme such that epithelium eventually permits mesenchyme to undergo osteogenesis (Bradamante and Hall, 1980; Dunlop and Hall, 1995; Francis-West et al., 1998; Hall, 1978; Hall and Coffin-Collins, 1990; Hall and Van Exan, 1982; Helms and Schneider, 2003; Merrill et al., 2008; Sharpe and Ferguson, 1988; Tyler and Hall, 1977; Tyler and McCobb, 1980; Vaglia and Hall, 1999; Van Exan and Hall, 1984; Wedden, 1987). When NCM is isolated from mandibles at an early stage (e.g., before Hamburger Hamilton (HH) stage 27) and cultured without epithelium, bone does not form (Dunlop and Hall, 1995; Merrill et al., 2008). However, mesenchyme collected from mandibles at later stages can form bone in the absence of the epithelium, meaning that mesenchyme is no longer dependent on osteogenic signals from the epithelium.

Mandibular bone formation initiates when mesenchymal cells start condensing at HH27. These mesenchymal condensations subsequently differentiate into osteoblasts by HH31 and undergo intramembranous ossification whereby they secrete extracellular matrix

products that produce osteoid, which is unmineralized bone tissue (Hall et al., 2014). Because the EMI required for bone formation appear to end by HH27, EMI may only be required for the initiation of osteogenesis but not for the subsequent maintenance of jaw development (Hall, 1978; Merrill et al., 2008; Tyler and Hall, 1977). In defining the nature of the EMI and the mechanistic contributions of each tissue, previous studies have suggested that the overlying epithelium plays a permissive role whereas the mesenchyme signals to the epithelium instructively (Hall, 1978, 1980, 1981; Hall, 1988; Schneider and Helms, 2003; Tyler and Hall, 1977). Evidence of the permissive role of epithelium comes from studies in which flank epithelium, which normally overlies non-osteogenic mesenchyme, can function in place of mandibular epithelium and sustain bone formation (Hall, 1978, 1981).

Trans-filter experiments have shown that unknown factors, which are secreted from the epithelium and deposited in the basal lamina, can induce bone (Hall, 1978, 1980, 1981; Hall et al., 1983; Tyler and Hall, 1977). Such results suggest that mandibular mesenchyme does not require a direct contact with the adjacent epithelium in order to become osteogenic, but rather is affected by proteins secreted from the epithelium prior to osteogenesis (Hall, 1982). When epithelial products are digested by protease treatment, mandibular mesenchyme is unable to form bone, indicating that the epithelial proteins are themselves osteogenic in nature (Hall and Van Exan, 1982). Moreover, these osteogenic proteins likely have a low molecular weight since they are still able to induce mesenchyme when they are exposed to filters with pore sizes that only allow secreted proteins to travel through (Hall and Van Exan, 1982).

While such experiments have helped characterize some of the expected properties of the epithelial proteins that regulate mandibular osteogenesis, what these tissue recombination studies have not demonstrated, however, is precisely when and from where the initial signals for osteogenesis arise, and more importantly, what those signals may be on the molecular level. To address this question, our laboratory has developed a chimeric transplant system that leverages the fact that quail and duck embryos undergo different rates of maturation (17 days versus 28 days from fertilization to hatching, respectively), and this feature enables us to test for the role of NCM during mandibular osteogenesis (Ealba et al., 2015; Fish and Schneider, 2014; Hall et al., 2014; Merrill et al., 2008).

Quail-Duck Chimeric System

Studies in our laboratory using chimeras between quail and duck embryos have revealed that NCM signals to epithelium instructively by establishing the timing of EMI and by regulating gene expression during the development of the beak, feathers, and bone (Eames and Schneider, 2005; Hall et al., 2014; Merrill et al., 2008; Schneider, 2005; Schneider and Helms, 2003). To generate a chimeric “quack” embryo, presumptive NCM destined to form the jaw skeleton is transplanted between quail and duck embryos that are stage-matched at HH9 (Fish and Schneider, 2014; Lwigale and Schneider, 2008). This is a stage when the neural tube is closing and neural crest cells are beginning their migration in the avian head region (Schneider, 1999). Because quail embryos develop faster than do duck embryos, the quail donor NCM in chimeric quack mandibles maintains about a three-stage faster timetable for bone formation within the slower environment of

duck hosts (Hall et al., 2014; Merrill et al., 2008). By examining the effects of the faster-developing quail NCM on the overlying slower-developing duck epithelium in comparison to those of a normal duck, we can tease apart the role of each tissue in mediating the EMI. From this work we have discovered that the EMI regulating osteogenic induction and condensation of mandibular NCM are not only completed in duck by HH27, but more importantly, that they are governed by NCM (Merrill et al., 2008). The overarching strategy for my project is to leverage the ability of quail donor NCM to regulate duck host epithelium as a way to screen for novel NCM-dependent factors that are secreted by mandibular epithelium. I can then test the extent to which such factors control bone formation in the developing lower jaw skeleton.

Our lab has previously and successfully used this experimental strategy to demonstrate that one important secreted protein that plays a role in directing the timing of mandibular osteogenesis is Bone Morphogenetic Protein 4 (BMP4) (Merrill et al., 2008). Such a conclusion is supported by four lines of evidence from our prior work. First, Bmp4 expression in the mesenchyme and epithelium of quack chimeras follows the accelerated timing of quail donor NCM, revealing that its expression is NCM-mediated. Second, exogenous application of recombinant BMP4 protein induces osteogenic markers and premature differentiation of osteoblasts compared to controls, which is consistent with previously reported experimental and clinical data for BMPs (Reddi and Cunningham, 1993; Toriumi et al., 1991; Wang et al., 1990; Wozney et al., 1988). Third, inhibiting BMP signaling results in a delay of bone formation. Fourth, analysis of candidate gene expression reveals that NCM regulates BMP signaling and osteogenic targets such as

Runx2, and that this regulation requires an interaction with the adjacent epithelium prior to HH24 but not beyond HH27, which is after the osteogenic EMI are no longer required.

However, while BMP4 appears to mediate the EMI required for bone formation, and BMP4 can induce limited amounts of bone in both experimental and clinical settings, our past experiments also reveal that BMP4 alone is not sufficient to induce NCM to form bone in the absence of epithelium. Therefore, other additional molecules likely play critical roles in the EMI that mediate mandibular osteogenesis. Identifying such molecules was the major goal of my project and to this end, I performed an RNA seq experiment designed to screen for NCM-mediated genes that are differentially expressed in mandibular epithelia between HH24 and HH27 (before and after osteogenic mesenchyme becomes independent of epithelia). The design, results, and analysis of this RNA seq experiment are described in Chapter 2. For the project described in Chapter 2, I collaborated with Dr. Jennifer Fish and Dr. Zuzana Vavrušová (while they were working in Dr. Schneider's laboratory) who performed the original quail-duck transplants and generated the RNA-seq dataset. For my part, I conducted all the analyses that identified novel candidate genes, and I performed all the experiments that validated the RNA-seq dataset. In Chapter 3, I detail an experimental strategy in which I collaborated with Dr. Daniel Chu (who is also working in Dr. Schneider's laboratory) so that I could test and validate a novel construct for over-expressing genes-of-interest that I identified in our screen. This construct, which has been published (Chu et al., 2020) and is publicly available (https://www.addgene.org/Richard_Schneider/), stably integrates an inducible promoter system that enables us to control precisely when and where we want a given gene to be

ectopically expressed at any stage of development. In Chapter 4, I investigate the role of two genes that were highly differentially expressed in my screen and met my other criteria for candidates that may mediate the epithelial-mesenchymal interactions required for mandibular osteogenesis. The work presented in Chapter 4 represents my own independent efforts. In Chapter 5, I summarize the major findings from my work and describe future directions and clinical implications. Overall, my thesis project has validated a novel strategy for identifying molecular mechanisms of mandibular osteogenesis and has uncovered new molecules that may have therapeutic implications for generating de novo bone in cases of birth defects, disease, and injury.

**Chapter 2: An Experimental Strategy Using RNA-seq To Identify Differentially
Expressed Epithelial Genes During Mandibular Osteogenesis**
(in collaboration with Dr. Jennifer Fish and Dr. Zuzana Vavrušová)

Introduction

The goal for this part of my project was to screen for NCM-dependent genes expressed in mandibular epithelia of duck and chimeric quck using a high-throughput and un-biased strategy. Our approach allowed for comparisons both between and among groups by accounting for the three-stage difference between quail donor and duck host cells in chimeric quck embryos (Fish and Schneider, 2014; Lwigale and Schneider, 2008; Schneider and Helms, 2003). Importantly, the mandibular epithelia that we analyzed were always derived from duck, which by design eliminated the noise of interspecific comparisons. In other words, the only meaningful differences in gene expression relevant to our hypothesis should be in those duck epithelia exposed to quail donor NCM.

Using previously published data from our lab and elsewhere on the timing of EMI that regulate mandibular osteogenesis (see Chapter 1 and references therein), we decided that the most applicable embryonic stages to screen for osteogenic factors secreted by mandibular epithelium would be duck HH24, duck HH27, and quck HH24. Again, HH24 quck contain quail donor NCM that are three stages ahead (i.e., HH27) of the duck host and thus we hypothesized that these donor NCM would differentially and prematurely regulate expression of NCM-dependent genes in duck host epithelium. Much prior work from our lab demonstrates that donor NCM regulates host gene expression in this exact manner and we know that HH24 and HH27 represent the embryonic stages before and after osteogenic mesenchyme becomes independent of epithelia (Ealba et al., 2015; Eames and Schneider, 2005, 2008; Hall et al., 2014; Merrill et al., 2008; Schneider and Helms, 2003; Smith et al., 2022; Tokita and Schneider, 2009).

To identify candidate genes, we utilized RNA-sequencing (RNA-seq), which is a high-throughput and un-biased technique that applies next-generation sequencing (NGS) to uncover and quantify the dynamic levels of all the mRNA (i.e., transcriptome) in a given sample (Wang et al., 2009). With our experimental design, RNA-seq would allow us to identify the totality of mRNA transcripts whose levels are normally changing in the epithelia of duck between HH24 and HH27, but also identify the subset of those epithelial mRNA transcripts that are regulated by NCM.

Our basic experimental strategy was to collect epithelia from duck HH24, duck HH27, and quack HH24, which we separated from the lower jaw primordia by using enzymatic digestion. We extracted total RNA from each sample, which we reversed transcribed into a library of cDNA. These cDNA libraries were then fragmented into short reads of 50 base pairs, enhanced, and attached with adaptors for a subsequent sequencing step. The resulting sequence reads were then aligned with the reference duck genome, thus allowing us to quantify the level of transcripts by quantifying the number of DNA reads.

To narrow the number of genes examined we used the following selection criteria: (a) genes that demonstrated a consistent fold change ($p < 0.05$) between replicates of duck and quack; (b) genes that changed by two-fold or greater; (c) genes that encode cytokines or other secreted molecules; (d) genes that are thought to be involved in osteogenesis; and (e) genes known and/or characterized. Based on these criteria, we identified numerous potentially relevant genes. Top candidates were confirmed with qPCR and *in situ* hybridization on whole mount embryos and tissue sections. While our approach

employs a powerful strategy to identify differentially expressed genes among tens of thousands of genes in the epithelia without biases, there are several caveats to consider. First, the duck reference genome that we are using to align our dataset contains some sequences in regions that remain poorly annotated in NCBI (<https://www.ncbi.nlm.nih.gov/datasets/genome/?taxon=8839>). Second, the technical process of DNA sequencing has inherent base-calling error rates and sequencing biases that may affect the accuracy of the alignments and read counts. Third, our specific experimental design does not rule out possible contamination of duck epithelial tissue by quail NCM that may remain adherent to the adjacent duck epithelium, which can further complicate the analysis by introducing quail transcripts into the dataset of quack chimeras. To account for these limitations, we verified all genes of interest individually by also aligning mRNA transcripts manually, by checking sequences for single nucleotide polymorphisms indicative of quail versus duck transcripts, and by using RT-qPCR to validate the changing levels of gene expression observed within and among experimental and control groups.

Our analyses identified numerous genes that are differentially expressed in the mandibular epithelia of Duck HH24 versus Duck HH27 epithelia. Our results include not only osteogenic candidates, but likely many other genes that undergo changes in expression in association with normal growth processes of development such as thickening and stratification of the mandibular epithelium as well as the formation of epithelial junctions as the tissue matures (Lucas and Stettenheim, 1972). Importantly, we also successfully identified a subset of genes that were differentially expressed in the

epithelia between Duck HH24 versus Quack HH24 epithelia, meaning that these genes were differentially regulated by faster developing quail NCM. Specifically, the union of the two datasets (i.e., Duck HH24 versus Duck HH27 and Duck HH24 versus Quack HH24) included several genes that met our selection criteria especially secreted molecules that may mediate EMI and have the potential to induce osteogenesis (**Figure 1**). We also performed a pathway analysis to confirm that these candidates may be osteogenic.

Materials and Methods

Incubation of Avian Embryos and Generation of Chimeras

Fertilized eggs of Japanese quail (*Coturnix coturnix japonica*) and white Pekin duck (*Anas platyrhynchos domestica*) were purchased commercially (AA Lab Eggs, Westminster, CA) and incubated at 37.8°C in a humidified chamber (GQF Hova-Bator 1588, Savannah, GA) until they reached embryonic stages appropriate for analyses. For all experiments, we adhered to accepted practices for the humane treatment of avian embryos as described in S3.4.4 of the AVMA Guidelines for the Euthanasia of Animals: 2013 Edition (Leary et al., 2013). Embryos were matched at equivalent stages the using the Hamburger and Hamilton (HH) staging system, a well-established standard that utilizes an approach based on external morphological characters, that is independent of body size and incubation time, and that can be adapted to other avian species such as quail and duck (Ainsworth et al., 2010; Fish and Schneider, 2014; Hamburger and Hamilton, 1951; Hamilton, 1965; Jheon and Schneider, 2009; Lwigale and Schneider, 2008;

Mitgutsch et al., 2011; Ricklefs and Starck, 1998; Schneider and Helms, 2003; Smith et al., 2015; Starck and Ricklefs, 1998).

For generating chimeras, quail and duck embryos were matched at stage HH9.5. Tungsten needles and Spemann pipettes were used for operations as described elsewhere (Fish and Schneider, 2014; Lwigale and Schneider, 2008; Schneider, 1999). Bilateral and unilateral grafts of rostral hindbrain and midbrain neural crest were made between quail and duck. Donor tissue were inserted into a host that had comparable regions of tissue removed. After surgery, chimeric embryos were incubated until HH24 (for quack chimeras) or HH24 and HH27 for duck controls.

Isolation of Mandibular Primordia and Epithelial Removal

Using forceps, mandibular primordia were cut along the proximal junction at each side of the maxillary primordia and placed into RNase-free ice-cold 1x PBS (BP3991, Fisher Scientific, Hanover Park, IL, USA). Epithelia from duck HH24, duck HH27, and quack HH24 (n = 3 for each group) were isolated from their adjacent mesenchyme. To separate epithelium from mesenchyme, trypsin (Sigma, T7409) and pancreatin (Sigma, P1625) were used to digest the basal lamina layer that connects epithelium and mesenchyme using a modified protocol based on previously published protocols (Tyler and Hall, 1977). Briefly, mandibles were rinsed in Ca²⁺/Mg²⁺ free PBS, and incubated for 20-30 minutes at 4°C in in 3:4 w/v trypsin:pancreatin solution in PBS. Digestion was stopped in 1:1 BGJb medium:FBS solution at 4°C, and mesenchyme was carefully separated from epithelium

using forceps. Epithelial removal was confirmed by inspection of each sample. Because these tissue layers are anatomically distinct, they can be easily distinguished.

RNA Extraction

For RNA extraction, isolated mandibular epithelia were transferred into 1.5 mL microcentrifuge tubes with as little 1x phosphate buffered saline (PBS) as possible. Samples for RNA extraction were flash frozen on dry ice in 100 % ethanol and stored at -80°C until ready to process. RNA was obtained from these samples using the Picopure Isolation RNA kit (ThermoFisher #KIT0204) and were processed for RNA-sequencing by the UCSF Functional Genomics Core.

RNA Sequencing, Data Alignment, and Normalization

RNA sequencing libraries were generated using TruSeq RNA sample prep kits with multiplexing primers, according to the manufacturer's protocol (Illumina). RNA sequencing was performed on HiSeq 2500 machines (Illumina). We multiplexed three samples per lane to ensure adequate depth of coverage. The analytic pipeline included de-multiplexing results, trimming adapter sequences from the reads, and aligning unique reads to the reference genome. Sequence alignment and splice junction estimation was performed using Bowtie2 and TopHat. For differential expression testing, genomic alignments were restricted to those mapping to the transcriptome provided by Ensembl Duck 1.0.

Pathway Analysis

QIAGEN Ingenuity Pathway Analysis was used to perform pathway analysis on the RNA-seq dataset. Genes that are differentially expressed by two-fold ($p < 0.05$) were fed into the pathway analysis module. Based on this input, the module generated a list of predicted networks of genes that belong to previously prescribed pathways. The top 10 pathways (ranked by confidence score) were selected.

Results

RNA-seq sequencing yielded ~322 million reads with an average read depth of 35.7 million reads/sample for those samples that were successfully sequenced (**Figure 2**). The alignment was done against the duck genome (Ensembl Duck 1.0) and those that mapped uniquely to known mRNAs were used to assess differential expression. The three quack samples displayed a lower mapping rate compared to duck HH24 and duck HH27 samples, indicating some possible contamination of the quack epithelia with mRNA from quail donor NCM. Candidate genes with suspected contamination arising from quail mRNA were manually aligned simultaneously to the duck genome vs quail genome using Geneious software (Geneious Prime, Version 2020.2.4) to sort out quail reads so that such contaminated could be eliminated.

mRNA profiles of quack HH24 were compared to duck HH24 and duck HH27. Candidate genes were selected from the overlap of two comparison groups including genes that encoded secreted-molecules that are differentially expressed between Duck HH24 versus Duck HH27 and Duck HH24 versus Quack HH24 with a threshold of two-fold

change or more ($p < 0.05$) as an initial screen (**Figure 3**). This first screening step yielded 287 genes, giving us a good number of genes to perform a pathway analysis using the Ingenuity Pathway Analysis software (QIAGEN). The top ten pathways identified include (ranked by order of differential expression): Role of Osteoblasts, Osteoclasts, and Chondrocytes; Regulation of the Epithelial-Mesenchymal Transition; Relaxin Signaling; NF- κ B signaling; Acute Myeloid Leukemia Signaling; Neurotrophin/TRK Signaling; CD40 Signaling; Bladder Cancer Signaling; IL-8 Signaling; and FGF Signaling (**Figure 4**).

In addition, and as described in Chapter 1, we focused on secreted proteins with low molecular weight to identify potential osteogenic candidates. (**Figure 5** and **Figure 6**). Importantly, one of the top differentially expressed genes that we identified was *Bmp4*, which as described in Chapter 1, is a known NCM-mediated osteogenic factor involved in the EMI required for mandibular osteogenesis. This result serves as an important internal control demonstrating that our quail-duck RNA-seq strategy indeed worked and gives us confidence in the ability to screen for other key differentially expressed genes that are NCM-dependent. In this context, we focused on two other secreted molecules that rose to the top of our list. The first was a gene called *C-X-C Motif Chemokine Ligand 14 (Cxcl14)* and the second was a member of a pathway that is known to be involved in osteogenesis, *Wnt-family member 11 (Wnt11)*. Both genes are described in more detail in Chapter 3 and Chapter 4, where I present results of my validation and gain- and loss-of function experiments.

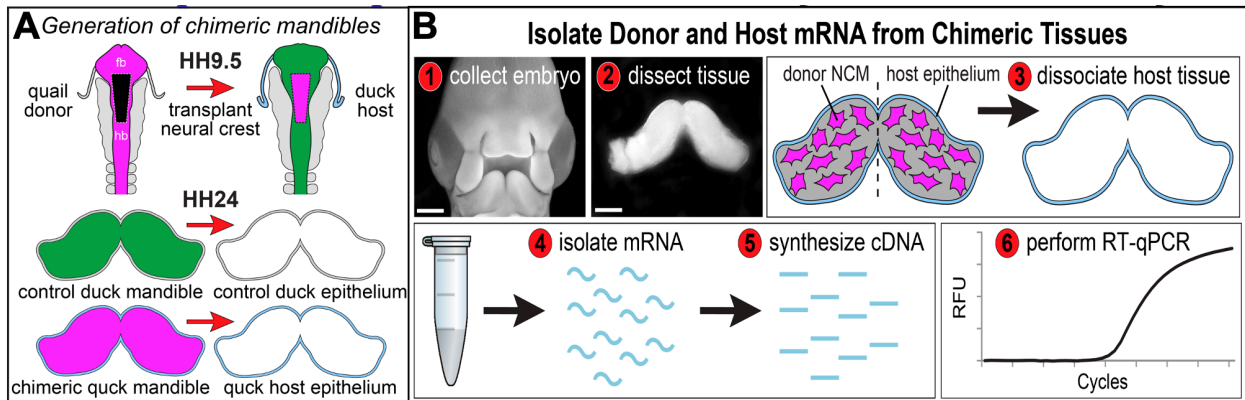


Figure 2.1: RNA seq experiment and RT-qPCR experiment to identify and validate expression of candidate genes.

(A) Neural crest cells are transplanted from quail into duck to make chimeric quack. Epithelial tissues are separated from the mesenchyme and collected for RNA extraction and RNA-seq. In quack mandibles, epithelia are host duck-derived but have been interacting with the adjacent faster developing donor quail NCM. (B) Steps in collecting epithelial tissues are identical in RNA-seq and in RT-pPCR experiments from step 1-5 when (1) embryos are collected at stage HH24 and HH27, (2) mandibular primordia are dissected, (3) epithelial tissue are collected, (4+5) RNA and cDNA are synthesized then either processed for RNA-seq or used in (6) RT-qPCR to analyze the gene expression level of candidate genes.

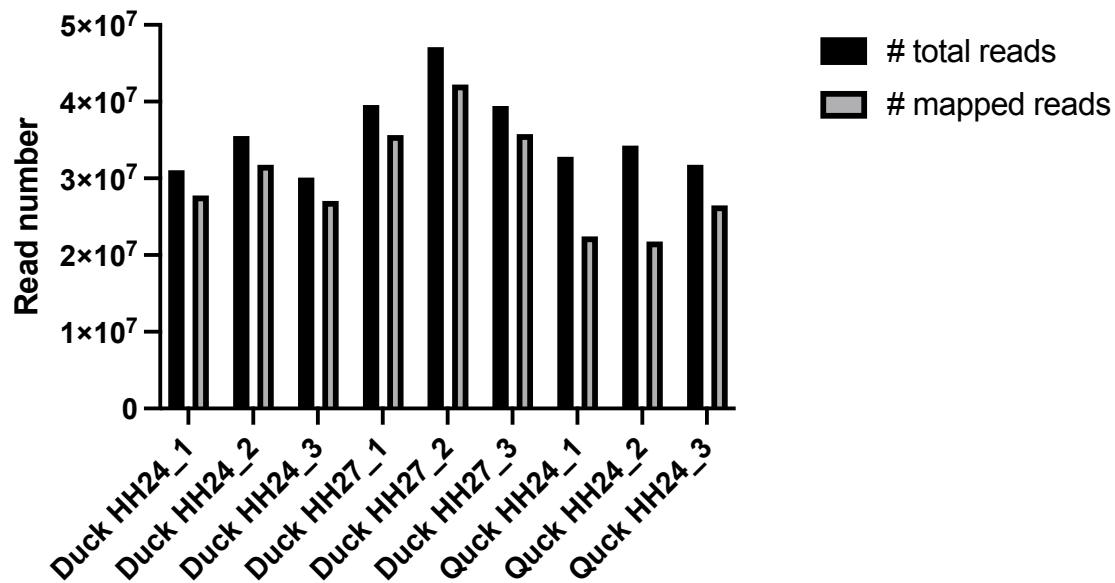


Figure 2.2: An overview of read coverage and mapped reads of the RNA-seq dataset.

Total number of reads versus number of reads successfully mapped to the published duck genome (Ensembl Duck 1.0). Number of reads across all three groups Duck HH24, Duck HH27, and Quck HH24 (n=3 each group) range from 300 million to 470 million reads. In Duck HH24 and Duck HH27 groups, more than 80% of reads are successfully aligned. In contrast, two out of three samples in Quck HH24 group have a lower number of aligned reads, possibly due to contamination from quail NCM RNA.

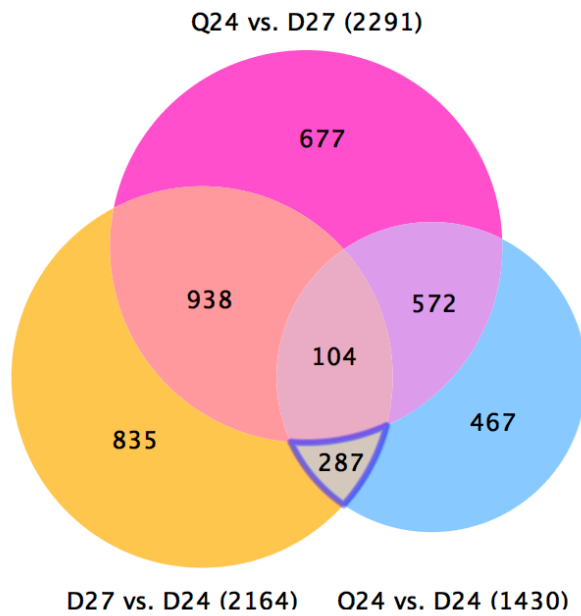


Figure 2.3: Venn diagram of differentially expressed genes.

The highlighted segment (including 287 genes) reflects the intersection between genes differentially expressed in Duck HH24 vs. Duck HH27 (D24 vs. D27) and Duck HH24 vs. Quack HH24 (D24 vs. Q24). Screening threshold used to generate this population of genes include two-fold change ($p < 0.05$).

Analysis Comparison 1

Canonical Pathway



Figure 2.4: Pathway analysis for differentially expressed genes.

Pathway analysis yielded potential pathways involved in differentially expressed genes in the epithelia during HH24-HH27.

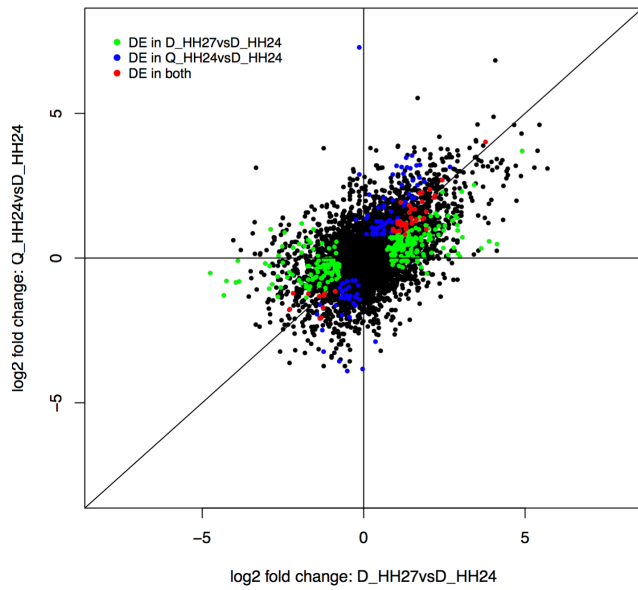


Figure 2.5: Log2 fold change graph for differentially expressed genes.

Differentially expressed gene when threshold is set at two-fold change or more. Candidate genes are represented as red dots, including genes that are both differentially expressed between Duck HH24 vs Duck HH27 and Duck HH24 and Quack HH24.

Name	D27 vs D24 Fold change	Q24 vs D24 Fold change	D24_1	D24_2	D24_3	D27_1	D27_2	D27_3	Q24_1	Q24_2	Q24_3
TXK	-10.25	-5.84	163	8	160	4	252	20	11	23	24
FGF8	-4.25	-3.94	220	284	262	73	52	53	41	73	52
BMP4	-2.7	-2.82	167	350	345	140	154	77	61	116	83
TMSB10	-2.3	-2.3	2459	3865	4231	906	2478	2390	1365	1304	3110
RPS29	-2.48	-2.24	1622	1779	2417	1009	2785	605	604	918	958
WNT2B	-2.19	-3.55	59	107	128	45	50	48	11	32	30
WNT11	-1.94	-1.4	504	751	688	309	449	407	348	593	285
FZD4	2.32	2.01	326	246	347	725	1227	788	636	458	483
BCHE	2.61	2.05	255	169	248	609	957	637	458	361	398
RHOBTB1	2.23	2.19	294	235	377	765	863	650	725	444	359
FAT4	2.31	2.21	1426	1001	1254	3174	4721	2856	2477	2366	1828
NFIA	2.95	2.34	327	351	265	1080	1135	876	633	672	496
SORCS1	2.46	2.37	197	289	285	534	676	810	488	580	596
ALDH1A2	2.33	2.38	294	233	179	605	1916	564	451	550	324
SESN3	2.74	2.42	480	500	552	1570	929	1374	1101	1085	771
OSBPL6	2.98	2.74	81	60	62	242	165	184	162	168	113
ANTXR1	4.07	3.57	203	139	180	726	662	785	533	572	377
KCNJ2	2.87	3.66	43	28	55	123	160	133	121	151	88
INPP4B	3.29	3.97	50	59	66	223	210	179	155	253	81
NFIB	2.25	4.09	166	122	102	344	658	277	477	475	262
CXCL14	5.92	4.14	381	65	193	1366	2846	1406	672	945	542
PDGFD	3.7	4.33	81	97	126	412	970	374	459	313	164
RELN	3.29	4.39	43	14	20	53	143	136	85	120	58
ADGRG6	3.31	6.4	116	132	126	415	446	460	718	690	229
SCN1A	5.58	7.64	14	1	2	11	37	64	30	52	16
NRXN1	4.34	9.4	21	34	32	164	306	97	178	302	71
ANGPTL1	4.42	9.64	17	2	3	23	47	51	55	77	17
DKK2	6.31	12.14	24	1	5	51	71	94	64	165	24
LVRN	17.54	13.86	3	2	2	57	31	33	28	32	7

Figure 2.6: List of identified candidate genes that are secreted molecules.

Identified candidate genes include genes that are differentially expressed in the epithelia of Duck HH24 vs Duck HH27 overlapping with Duck HH24 vs Quack HH24 with a minimum two-fold change. Only genes that encode secreted molecules. Raw data of each sample from three groups Duck HH24 (D24_1, D24_2, and D24_3), Duck HH27 (D27_1, D27_2, and D27_3), and Quack HH24 (Q24_1, Q24_2, and Q24_3) are shown.

**Chapter 3: An Experimental Strategy For Mis-Expressing Genes-of-Interest Using
Stable Integration of An Inducible Promoter System**

(in collaboration with Dr. Daniel Chu)

Introduction

Precisely altering gene expression is critical for understanding molecular processes of embryogenesis. Although some tools exist for transgene misexpression in developing chick embryos, we have refined and advanced them by simplifying and optimizing constructs for spatiotemporal control. To maintain expression over the entire course of embryonic development we use an enhanced *piggyBac* transposon system that efficiently integrates sequences into the host genome. We also incorporate a DNA targeting sequence to direct plasmid translocation into the nucleus and a D4Z4 insulator sequence to prevent epigenetic silencing. We designed these constructs to minimize their size and maximize cellular uptake, and to simplify usage by placing all the integrating sequences on a single plasmid. Following electroporation of stage HH8.5 embryos, our tetracycline-inducible promoter construct produces robust transgene expression in the presence of doxycycline at any point during embryonic development *in ovo* or in culture. Moreover, expression levels can be modulated by titrating doxycycline concentrations and spatial control can be achieved using beads or gels. Thus, we have generated a novel, sensitive, tunable, and stable inducible-promoter system for high-resolution gene manipulation *in vivo*. This construct allowed me to test the function of candidate genes identified in my RNA-seq experiment (Chapter 2), determine the extent to which such genes mediate the EMI during mandibular osteogenesis, and evaluate if they can induce bone. As a proof-of-concept, we cloned *Cxcl14* into our inducible-promoter system and tested if we could achieve robust over-expression in chick fibroblast cells, in mandible cultures, and *in ovo*.

Materials and Methods

The Use of Avian Embryos and Cell Culture

Fertilized eggs of chicken (*Gallus gallus*) and duck (*Anas platyrhynchos*) were purchased from AA Lab Eggs (Westminster, CA) and incubated at 37.5 °C in a humidified chamber (GQF Hova-Bator, Savannah, GA, 1588) until they reached embryonic stages appropriate for manipulation and/or analyses. Staging, collection, and humane handling of avian embryos was as performed as described in Chapter 2.

Embryonic chick fibroblasts (DF-1) were purchased (ATCC, CRL-12203) and cultured in Dulbecco's Modified Eagle's Medium (DMEM, Corning, 10-013-CV) supplemented with 10% FBS (VWR, 97068-085, Lot# 283K18) and 1X penicillin-streptomycin (ThermoFisher, 15140122) at 37 °C with 5% CO₂. Cells were passaged twice a week.

Cloning Coding Sequences

Full length cDNA synthesis from RNA was carried out using Maxima H-reverse transcriptase (ThermoFisher, K1651) following the manufacturer's directions with 2 µg of total RNA and 100 pmol of d(T)₂₀ VN primer. The cDNA synthesis reaction was carried out at 50 °C for 30 min, 55 °C for 10 min, 60 °C for 10 min, 65 °C for 10 min, and 85 °C for 5 min. Full length *Cxcl14* was amplified by PCR using Q5 Hot Start High-Fidelity DNA Polymerase (NEB, M0493L) and cloned using CloneJET PCR Cloning Kit (ThermoFisher, K1231). Following confirmation of cloning of full-length coding sequences by Sanger sequencing, *Cxcl14* was cloned into pEPIC1.1 digested with AflIII (NEB, R0520S) and EcoRI (NEB, R3101S) or pPIDNB digested with AflIII (NEB, R0520S) and PstI (NEB,

R3140S) using NEBuilder HiFi DNA Assembly Master Mix. All constructs were verified by Sanger sequencing and midiprep for electroporation and transfection using PureLink Fast Low-Endotoxin Midi Kit (Invitrogen, A36227).

Transfections and Electroporations

Cells were transfected with lipofectamine 3000 (ThermoFisher, L3000008) according to the manufacturer's instructions. Transfections for integrating *piggyBac* vectors were carried out in 6-well plates with 5 µg *piggyBac* plasmid, 5 µg of pNano-hyPBase, and 20 µl of P3000.

Electroporations were performed by injecting a solution of pEPIC1.1-Cxcl14 and pNano-hyPBase at 3 µg/µl and 1 µg/µl, respectively, with a small amount of Fast Green dye. DNA was injected with a Pneumatic PicoPump (PV830, World Precision Instruments) into dissected HH21 mandibular primordia using thin wall borosilicate glass micropipettes (O.D. 1.0 mm, I.D. 0.75 mm, Sutter Instrument, B100-75-10) pulled on a micropipette puller (P-97 Flaming/Brown, Sutter Instrument). Mandibles were placed between two gold plate electrodes 0.5 cm apart submerged in Hanks' balanced salt solution (Sigma-Aldrich). Electroporations were carried out by delivering five square pulses at 25 V for 50 ms spaced 500 ms apart (CUY21EDITII Next Generation Electroporator, BEX CO, Ltd). Mandibles were then cultured in BgJB medium (ThermoFisher, 12591038) supplemented with 10% FBS (VWR, 97068-085, Lot# 283K18) and 1 X penicillin-streptomycin (ThermoFisher, 15140122).

In ovo electroporations were performed using a solution of pPIDNB and pNano-hyPBase at 3 $\mu\text{g}/\mu\text{l}$ and 1 $\mu\text{g}/\mu\text{l}$, respectively. With the addition of Fast Green tracer dye, DNA solution was injected into HH8.5 chick neural tubes with a Pneumatic PicoPump using thin wall borosilicate glass micropipettes pulled on a micropipette puller. Platinum electrodes were positioned on each side of the area pellucida, centered on the midbrain-hindbrain boundary. For unilateral electroporations, we delivered three square pulses at 50 V for 1 ms spaced 50 ms apart followed by five square pulses at 10 V for 50 ms spaced 50 ms apart. For bilateral electroporations, we delivered three square pulses at 50 V for 1 ms spaced 50 ms apart, three square pulses at 50 V for 1 ms spaced 50 ms apart in the reverse polarity, three five square pulses at 10 V for 50 ms spaced 50 ms apart followed by, five square pulses at 10 V for 50 ms spaced 50 ms apart in the reverse polarity.

Doxycycline Treatment

Stock solutions of doxycycline hyclate (Acros Organics, 446060250) were made to a final concentration of 1 mg/ml in water, filter sterilized, and stored at $-20\text{ }^{\circ}\text{C}$ as single use aliquots. For *in ovo* treatments, 2.5 μl (for chick) and 3.75 μl (for duck) of the 1mg/ml dox stock solution was diluted with 750 μl of HBSS. This solution was then gently pipetted into the egg adjacent to the embryo and allowed to diffuse.

RNA Extractions

RNA was extracted from DF-1 cells and HH27 chick heads and/or mandibles using the RNeasy Plus Kit (Qiagen, 74136) following the manufacturer's directions. Whole heads

and DF-1 cells were resuspended in 600µl of RTL plus buffer supplemented with 1% β-mercaptoethanol. Homogenization was carried out in a Bead Mill 24 (ThermoFisher, 15-340-163) at 5 m/s for 30 s. Following purification of total RNA, residual genomic DNA was removed using TURBO DNA-free Kit (Invitrogen, AM1907).

Quantitative PCR

DNased RNA was reverse-transcribed using iSCRIPT (Bio-Rad, 1708841). Gene expression was quantified by qPCR with iQ SYBR Green Supermix (Bio-Rad, 1708882) and normalized to 18S rRNA following previously published protocols (Dole et al., 2015; Smith et al., 2016). Primer sets were designed and optimized as described previously (Ealba and Schneider, 2013) and are listed in below. Each sample was assayed in technical duplicate.

qPCR primers:

CXCL14 F3 Chick 5'-GCAGAAGGAGTAAAGTGCAA-3'

CXCL14 R3 Chick 5'-GTACCACTTGAGCAGCCTCA-3'

Cloning primers:

CXCL14 5UTR C F1 DC 5'-GAACACAAGACAGAACCCCG-3'

CXCL14 3UTR U R1 DC 5'-GGTGTGAAATCTGAAGTGCA-3'

Western Blot

DF-1 cells were lysed with 1X RIPA lysis buffer (EMD Millipore, 20-188) containing Halt protease inhibitors (ThermoFisher, 78430). A BCA assay (ThermoFisher, 23225) using a SpectraMax M5 plate reader was performed to quantify protein, and 40 µg protein was

electrophoresed on a 10% SDS polyacrylamide gel following a published protocol (Smith et al., 2016). Proteins were transferred to an Immobilon-PPVDF membrane (Millipore, Billerica, MA, IPVH00010). Membranes were probed with rabbit anti-chick RUNX2 primary antibody (1:1000, AbCam Burlingame, CA, Cat #ab23981), custom made rabbit anti-chick MMP13 antibody (1 μ g/ml, Genscript), rabbit anti-CXCL14 (0.2 μ g/ml, Peprotech, 500-P237), mouse anti-chick β -actin antibody (1:4000, Novus Biologicals, NB600-501), goat anti-rabbit IRDye 800CW (1:15000, LI-COR #925-32211), and donkey anti-mouse IRDye 680RD antibody (1:15000, LI-COR #925-68072). Fluorescent signal was captured using the Odyssey Imaging System (ThermoFisher). Quantifications of protein bands were normalized to β -actin (Image Studio Lite).

Imaging

DF-1 cells and embryonic tissues were imaged using a macroconfocal (Nikon AZ100 C2+). Timelapse experiments were carried out in a custom-made stage top incubator (Okolab) set to 37°C, 95% humidity and 5% CO₂. All DF-1 experiments were carried out in 6-well plates (Falcon, 08-772-1B) with 2 ml of DMEM.

Statistical Analysis

Statistical analysis carried out using Student's t-test was performed (GraphPad Prism version 8.4.3, GraphPad Software, La Jolla, CA). When multiple comparisons were made, p-values were adjusted using the Holm–Bonferroni method (Holm, 1979).

Results

CXCL14 Over-Expression Using pEPIC1.1

Chick *Cxcl14* full length (297 bp) was cloned into a vector that we developed called pEPIC1.1. We first confirmed that pEPIC1.1 constructs could overexpress *Cxcl14* by transfecting them into a chick fibroblast cell line (DF-1). pEPIC1.1-*Cxcl14* was able to induce strong overexpression compared to empty vector (**Figure 8**). The pEPIC1.1-*Cxcl14* construct increased *Cxcl14* mRNA levels $59,000 \pm 16,000$ times by qPCR ($p < 0.02$) and the CXCL14 protein levels 32 ± 4.6 times by WB compared to pEPIC1.1 ($p < 0.005$) (**Figure 8**).

We next confirmed that the pEPIC1.1 construct is functional at the tissue level. Mandibular primordia were dissected from HH24 chick embryos, injected with a plasmid solution containing pEPIC1.1-*Cxcl14* with or without hyPBase, and then electroporated. Mandibles were then cultured over seven days. After five days of culture, mandibles electroporated with pNano-hyPBase retained strong GFP expression while mandibles without pNano-hyPBase had greatly reduced expression compared to one-day post-electroporation (**Figure 7**). After seven days of culture mandibles electroporated without pNano-hyPBase had no detectable GFP expression.

CXCL14 Over-Expression Using pPIDNB

We generated the pPIDNB (*p*iggyBac, *i*nsulator, *D*T_S, m*N*eongreen, *b*i-directional) construct as a minimal dox-inducible plasmid. This plasmid is a modified version of

pEPIC1.1 but instead of constitutively expressing the gene of interest, it carries the reverse tetracycline transactivator (rtTA) that once bound to dox will activate the bidirectional tet promoter driving the gene of interest and the fluorescent mScarlet reporter gene.

We tested the ability of pPIDNB to drive exogenous gene expression by cloning in the coding sequence for *Cxcl14*. We first transfected DF-1 cells with pPIDNB-*Cxcl14*, treated with various doses of dox, and found that *Cxcl14* expression correlated with the concentration of dox (**Figure 9A**). These results along with the RFP data above indicate that dox dose-response is tunable at the cellular level and not simply a binary response to increased dox concentrations causing more cells to express RFP. We found DF-1 cells treated with 2.5, 10, 50, and 250 ng/ml dox for 24 hours increased *Cxcl14* mRNA expression by 27 ± 6.4 ($p < 0.05$), 96 ± 23 ($p < 0.05$), 149 ± 34 ($p < 0.05$), and 178 ± 20 ($p < 0.005$) times respectively, compared to cells not treated with dox. WB analysis also showed a dose response with 2.5, 10, 50, and 250 ng/ml dox with CXCL14 protein levels increasing by 6.3 ± 0.053 ($p < 0.005$), 12 ± 3.8 ($p < 0.05$), 15 ± 1.6 ($p < 0.005$), and 17 ± 1.9 ($p < 0.005$) times respectively, compared to cells not treated with dox (**Figure 9B**).

Discussion and Conclusion

To achieve robust over-expression of *Cxcl14* in cells and in embryonic tissues, we generated an “all-in-one” *piggyBac* dox-inducible system. Our experimental strategy was successful for several reasons. First, the pPIDNB plasmid was designed to be as small as possible to optimize cellular uptake while incorporating critical features to maximize its

functionality. Second, the DTS and insulator sequences served to promote expression by directing nuclear entry of the plasmid and by blocking heterochromatic silencing expression. Third, we used mutated *piggyBac* and hyPBase sequences to increase genome integration efficiency. Fourth, we also incorporated a constitutively expressed GFP to mark cells that have taken in plasmid DNA and RFP to mark dox-induced cells. Overall, we have shown that our system facilitates precise temporal control of gene induction and can be easily adapted for *in vitro* or *in ovo*. Spatial control of gene expression was achieved by electroporating regions of interest and/or by applying beads or gels to localize the distribution of dox.

Our pPIDNB system was able to induce expression quickly and its reliance on a low dose of dox is important because dox has biological effects beyond antimicrobial activity including affecting matrix metalloproteinase activity, inflammation, the NF- κ B pathway, and the nervous system (Alexander-Savino et al., 2016; Bahrami et al., 2012). High concentrations of dox (e.g., 1000 ng/ml) are cytotoxic in culture and have strong proliferative and metabolic effects, and some cell types are affected at even lower concentrations (e.g., 100-200 ng/ml) (Ahler et al., 2013; Alexander-Savino et al., 2016; Ermak et al., 2003). By using a low dose of dox (50 ng/ml) we have likely minimized any off-target effects of dox treatment.

While in the current study, we designed the pPIDNB construct for transgene overexpression, we envision that future applications will include different types of experiments such as gene knockdown using CRISPRi (Mandegar et al., 2016; Qi et al.,

2013). For example, catalytically inactive *Cas9* could be placed with transcriptional repressors under an inducible tet promoter (Qi et al., 2013; Yeo et al., 2018). Constitutively active U6 promoters would drive expression of single guide RNAs (Cong et al., 2013; Gandhi et al., 2017; Williams et al., 2018). Overall, a great strength of avian model systems has been the combination of experimental embryology and modern genetic techniques. This new, sensitive, stable, and robust inducible-promoter system that we developed builds on this strength and joins an arsenal of tools for manipulating gene expression that benefits the broader developmental biology community.

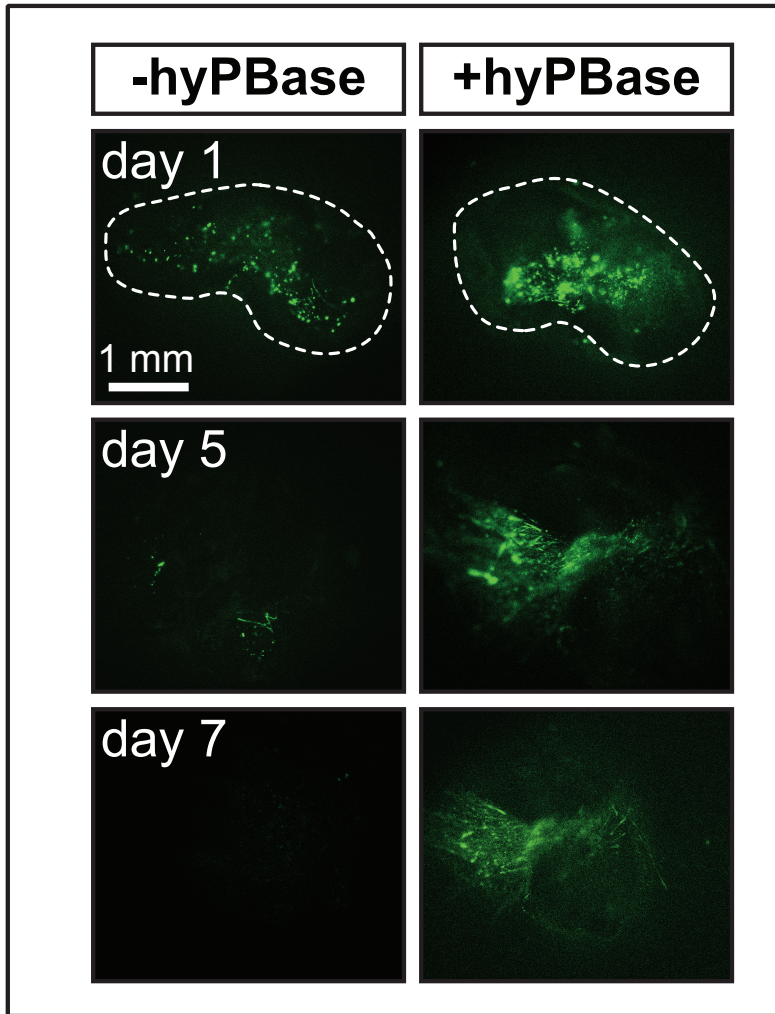


Figure 3.1: Time course imaging of HH21 chick mandibular primordia overexpressing *Cxcl14*.

Fluorescent images showing a time course of HH21 chick mandibular primordia electroporated with pEPIC1.1- *Cxcl14* either without pNano-hyPBase (left column) or with (right column) cultured, and imaged at day 1, 5, and 7.

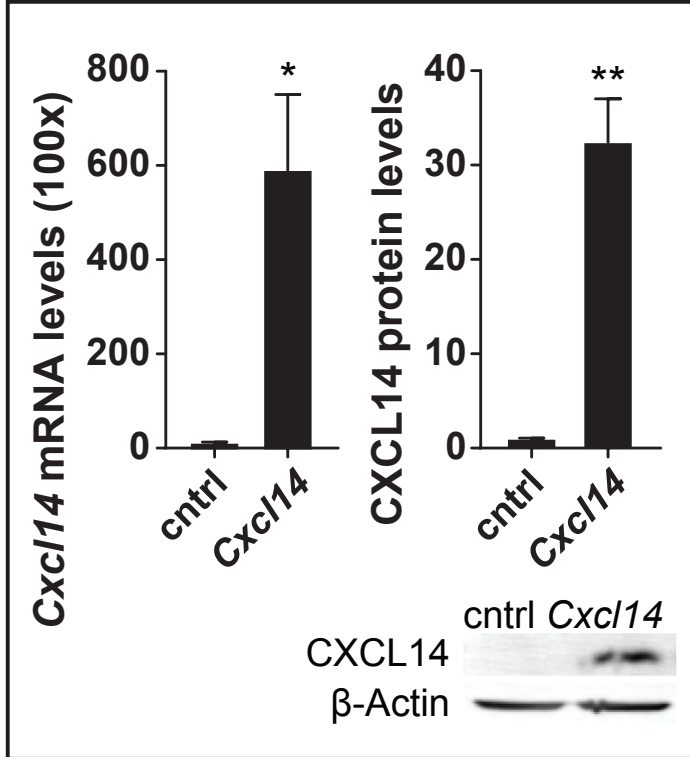


Figure 3.2: Validation of successful overexpression of pEPIC1.1-*Cxcl14*.

Cxcl14 with pEPIC1.1. DF-1 cells were transfected with control (cntrl) empty pEPIC1.1 or pEPIC1.1 plus *Cxcl14* coding sequence and harvested 3 days post-transfection. Relative mRNA levels were measured by qPCR and normalized using 18S. Relative protein levels were measured by western blot (WB) and normalized using β-Actin. Representative WBs are shown below. There were two biological replicates for *Cxcl14*. All qPCR was performed in technical duplicate. A two-tailed t-test was used for all statistical analyses. Error bars represent standard error of the mean (s.e.m.). (* $p < 0.05$; ** $p < 0.005$).

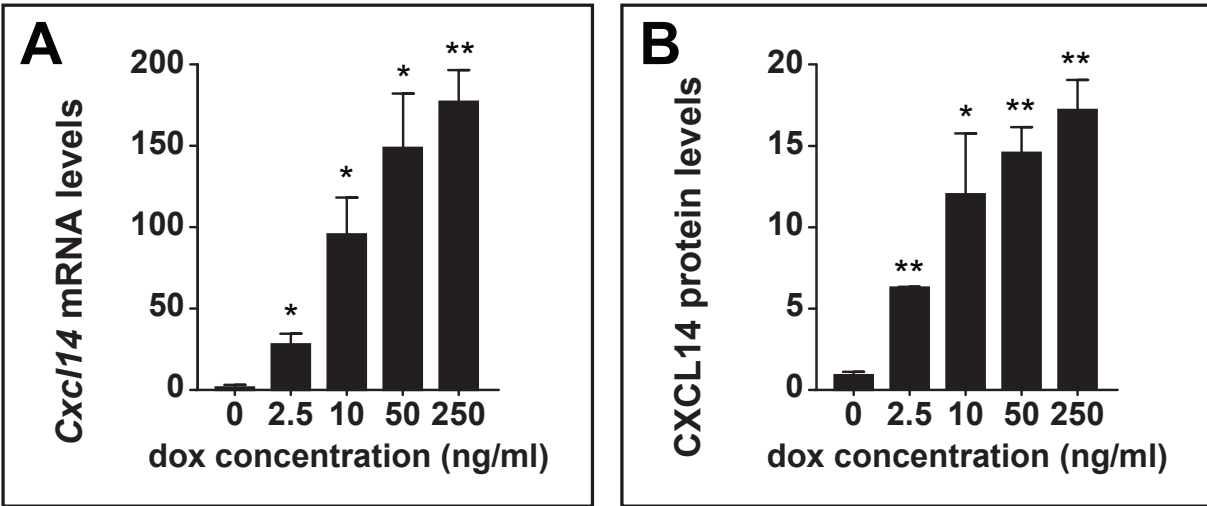


Figure 3.3: Validation of successful overexpression of pPIDNB-*Cxcl14*.

CXCL14 overexpression levels using pPIDNB plasmid. (A) Dox induction was measured in DF-1 cells on the mRNA level. There are three biological replicates for each group. (B) Dox dose response of protein levels for *Cxcl14*. There are three biological replicates for each group except for the 2.5 ng/ml treatment, which has two biological replicates. All qPCRs were performed in technical duplicate. A two-tailed t-test was used for all statistical analyses. When multiple comparisons were made, p-values were adjusted using the Holm–Bonferroni method. All bar graphs are shown as mean \pm s.e.m. (* $p < 0.05$; ** $p < 0.005$).

**Chapter 4: A Role for CXCL14 and WNT Signaling in Mediating the Epithelial-
Mesenchymal Interactions Required for Mandibular Osteogenesis**

Introduction

The goal of my project was to identify and test for osteo-inductive epithelial factors regulated by NCM in an in vivo context. My results have the potential to be highly relevant for creating new strategies to treat craniofacial defects that involve a bone deficiency. Past studies in our lab and others have shown that members of the BMP family have osteogenic potential (Merrill et al., 2008). However, clinically, BMPs fail to induce significant amounts of bone when used with autologous bone grafts as compared to controls. This limited clinical success is likely due to an incomplete understanding of the totality of factors required to promote bone growth during development. Similarly, work from our lab has shown that while BMP4 is osteoinductive, BMP4 alone cannot function in place of epithelium during the EMI required for mandibular osteogenesis. Thus, there is likely a combination of molecules that work together to induce bone formation in mandibular mesenchyme.

The Role of CXCL14 During Mandibular Osteogenesis

Based on the properties for “proteins of interest” as predicted by the tissue recombination experiments described in Chapter 1 and Chapter 2 (i.e., small, secreted, and low molecular weight), we focused on chemokines, which are a large family of small proteins (8-10kDa) that include at least 50 chemokine ligands and 19 functional receptors (Proudfoot, 2002). Our RNA-seq experiment identified CXCL14 as a potential candidate gene for mediating the mandibular EMI between stages HH24 and HH27. CXCL14 is a small chemokine that belongs to the CXC protein subfamily, and its receptor remains uncharacterized. However, CXCR4, the known receptor of CXCL12, has been found to

have direct interaction with CXCL14. CXCL14 may compete with CXCL12 in binding to CXCR4 and act as a decoy ligand that blocks CXCL12 signaling. Binding between CXCL12 and CXCR4 appears to trigger organogenesis, hematopoiesis, and angiogenesis during development (Collins et al., 2017; Hara and Tanegashima, 2014; McGrath et al., 1999; Tachibana et al., 1998; Zou et al., 1998). However, the functions of various CXC ligands in development are still not well understood but there are studies indicating their important roles in metabolism, cancer, and immunology.

For example, CXCL14 appears to regulate neurovascular development of the retina (Ojeda et al., 2013). Knockdown of CXCL14 in a chick model using RCAS-shRNA results in defects in retinal neurogenesis and causes ectopic vascularization of the cornea (Ojeda et al., 2013). Another possible role for CXCL14 during embryonic development is in the regulation on tendon differentiation during chick limb development where CXCL14 can activate expression of the tendon marker scleraxis (Scx) in vitro and its expression overlaps with Scx in limb connective tissues (Nassari et al., 2017). Interestingly, especially in the context of the differentially expressed genes that I observed in my RNA-seq analysis (**Figure 3**), CXCL14 is found to be regulated by BMP and WNT signaling (Nassari et al., 2017; Park et al., 2009).

CXCL14 has also been shown to affect metabolism by attracting macrophages in white adipose tissue and thus can regulate the sensitivity of fat cells to insulin (Hara and Nakayama, 2009; Nara et al., 2007). Mice deficient in CXCL14 that are fed with a high fat diet cannot mobilize macrophages in white fat cells and thus display an improved ability

to secrete insulin (Hara and Nakayama, 2009; Nara et al., 2007). In contrast, obese mice show increased expression of CXCL14, which correlates with their lack of insulin response and high levels of blood sugar and fat. In addition, homozygous CXCL14^{-/-} female mice have a more pronounced phenotype than their male counterparts in terms of insulin insensitivity (Hara and Nakayama, 2009; Nara et al., 2007).

CXCL14 is also associated with cancer and cancer progression. For example, CXCL14 has been found to be dysregulated in multiple types of cancers such as cervical, colorectal, endometrial, and head and neck carcinomas (Westrich et al., 2020). Increased levels of expression of stromal CXCL14 are correlated with increased metastasis resulting in poor prognosis (Westrich et al., 2020). In contrast, some other studies report that downregulation of CXCL14 is associated with many cancers including cervical, prostate, lung, pancreatic, gastric, and oral cancers (Westrich et al., 2020). Thus, CXCL14 can function both as a tumor suppressor or tumor promoter in a context-dependent manner.

Similar to the functions of other chemokines during chemotaxis, CXCL14 can signal to and activate dendritic cells (Westrich et al., 2020), natural killer cells (Aaboe et al., 1995), and CD8⁺ T-cells (Kumar et al., 2022). Other important roles of CXCL14 in the immune system have been described, including angiogenesis, immune surveillance, and antimicrobial activity (Lu et al., 2016).

Several groups have reported that homozygous CXCL14^{-/-} mice appear healthy and develop normally with no gross abnormalities in various organs including intestine,

kidney, lung, and lymph node. Interestingly, despite no obvious phenotype, homozygous CXCL14^{-/-} are 12-20% lighter than their wild-type littermates, and litters of intercrossing of heterozygous parents skewed the expected Mendelian frequency for CXCL14^{-/-} homozygotes to 10.3% instead of 25% (Hara and Nakayama, 2009; Meuter et al., 2007; Nara et al., 2007). CXCL14 likely has functional redundancy and thus a single chemokine deletion has no discernible effect on immune function. Several studies suggest the chemokine CXCL12 is most closely related to CXCL14 and therefore has likely evolved together with CXCL14 and shares the same signaling axis that compensates when CXCL14 is mutated or absent (Hara and Tanegashima, 2014; Lu et al., 2016; McGrath et al., 1999; Tachibana et al., 1998; Zou et al., 1998).

Gene and Protein Structure of CXCL14 and Its Expression During EMI

CXCL14 possesses a “CXC” motif, which has four conserved cysteine residues that form disulfide bonds. The N-terminus is strongly hydrophobic and its first 22 amino acids appear to act as a signal peptide that is cleaved prior to secretion (Westrich et al., 2020). CXCL14 is conserved during evolution from fish to humans (Hara and Tanegashima, 2014). Duck, quail, and chick CXCL14 protein sequences are very well conserved (sharing over 90% homology) except for the duck sequence, which lacks the signal peptide (**Figure 10**). Our RT-qPCR and *in situ* hybridization analyses validate that *Cxcl14* is expressed in mandibular mesenchyme and epithelium of chick, quail, and duck during EMI. We also find that *Cxcl14* is expressed in adjacent and overlapping domains with other ligands such as *Wnt11* that are known to play a role during osteogenesis and become highly differentially expressed in our RNA-seq screen. This finding suggests that

signaling by CXCL14 and WNT11 may work in tandem to mediate the EMI required for mandibular osteogenesis. Thus, we set out to test the hypothesis that epithelial signaling by CXCL14 and WNTs govern the timing of EMI required for bone formation in the mandible.

WNT Signaling and Bone Formation

WNT ligands are secreted glycoprotein growth factors that act via canonical or non-canonical pathways and exert a broad variety of effects in cells. The canonical WNT pathway acts via binding of WNT ligands to the Fzd-LRP5/6 receptor complex, which induces the activation of Disheveled (Dvl). Dvl inhibits the proteosomal degradation of phosphorylated β -catenin, allowing β -catenin to translocate to the nucleus. Once inside the nucleus, β -catenin binds to TCF/Lef1 transcription factors, which activate genes important for cell differentiation. The non-canonical WNT pathway acts via receptors different than the Fzd-LRP5/6 receptor complex, including the calcium-dependent pathway and the planar cell polarity pathway (Dann et al., 2001; Wodarz and Nusse, 1998).

Components of the WNT signaling pathway have been found to play an important role in osteogenesis (Haxaire et al., 2016; Vlashi et al., 2023). For example, the planar cell polarity pathway mediates the organization of the cytoskeleton via activation of RhoA and ROCK (Goldstein et al., 2006), which have been found to be associated with osteogenic differentiation (Arnsdorf et al., 2009). Axin, a member of the canonical WNT pathway, can modulate WNT transduction signal either via stabilizing the β -catenin destruction complex

to promote β -catenin degradation and thus inhibit WNT signaling, or via interacting with LRP5/6 receptor to promote WNT signaling (Song et al., 2014). Axin 2^{-/-} mice have reduced limb length (Dao et al., 2010), increased bone mass (Yan et al., 2009), and increased intramembranous ossification in the skull (Yu et al., 2005).

The importance of the WNT pathway in endochondral and intramembranous bone formation has been described (Jiang et al., 2014; Leucht et al., 2008), yet the exact role of WNT ligands and their downstream targets is highly complex and context-dependent. In this study, we perform experiments that modulate both the canonical and non-canonical WNT pathways, and we demonstrate that WNT is a positive mediator of the EMI required for osteogenesis. We also shown for the first time that these EMI likely involve combinatorial signals by CXCL14 and the WNT pathway that regulate bone formation in the lower jaw.

Materials and Methods

Organ Culture

To separate epithelium from mesenchyme, trypsin (Sigma, T7409) and pancreatin (Sigma, P1625) were used following published protocols to digest the basal lamina layer that connects epithelium and mesenchyme (Tyler and Hall, 1977). The procedures of culturing mesenchyme or whole mandibles were carried out as we have done previously (Merrill et al., 2008). Briefly, each sample of isolated mesenchyme was positioned on a Millipore filter (0.8 μ m porosity, 125-150 μ m thickness, Sigma, AABP04700), placed in a

well of a 12-well insert plate (VWR, 734-3262), and submerged in BGJb (Thermo, 12591038) with 10% fetal calf serum (VWR, 97068-085, Lot# 283K18). Cultures were incubated at 37°C for 24 hours or up to seven days then assayed for gene expression or processed for histology analysis.

Preparation of Micropipettes

Micropipettes for DNA injection were generated using a micropipette puller (model P-87 Flaming/Brown, Sutter Instrument Co., Novato, CA, USA). Borosilicate capillary glass without a filament and with an outside diameter of 1 mm and an inner diameter of 0.75 mm (B100 – 75 – 10, Sutter Instrument Co., Novato, CA, USA) was used. Program settings were as follows: Heat = 693, Velocity = 50, Pull = 100, Time = 250, Press = 300.

Mandibular Electroporation

Platinum electrodes were fixed onto a microscope glass slide. The anode and cathode were placed 0.5 cm apart. 3 µl of a solution including the inducible expression vector pEPIC (3 µg/µl) and a small amount of Fast Green dye were loaded into a pulled glass micro-injection needle. Two to three injections were made 1 mm deep into the tissue, and the contralateral side was injected with an empty pEPIC. Current was applied using three square pulses at 65 V for 1 ms spaced 50 ms apart in the reverse polarity using the BEX CUY21EDITII Pulse Generator (CUY21EDIT2, BEX CO., LTD, Tokyo, Japan).

Histology and Bone Quantification

Mandible cultures were fixed in 4% paraformaldehyde (PFA) (Electron Microscopy Sciences, Hatfield, PA, USA) overnight at 4°C (Schneider et al., 1999; Schneider et al., 2001). To detect bone deposition in sections, embryos were dehydrated in methanol, embedded in paraffin, and cut into 10 µm sagittal sections. Sections were deparaffinized, rehydrated, and adjacent sections were stained with Milligan's trichrome at room temperature as previously described (Eames and Schneider, 2005; Hall et al., 2014; Presnell et al., 1997; Schneider et al., 2001; Solem et al., 2011; Tokita and Schneider, 2009). Briefly, sections were stained in 1% acid fuchsin for 30 seconds followed by 1% phosphomolybdic acid for 2 minutes, 2% orangeG for 30 seconds, 1% acetic acid for 2 minutes, 1% aniline blue for 3 minutes, and 1% acetic acid for 3 minutes. Slides were dehydrated in ethanol and mounted in Cytoseal (Thermo Scientific, 8310-4) with a glass coverslip.

Osteoid staining was performed as previously described (Merrill et al., 2008; Rális and Rális, 1975). Briefly, deparaffinated sections were re-hydrated through an ethanol series, washed with saturated picric acid for 30 seconds, 1% phosphotungstic acid for 5 minutes, quickly rinsed with 1% acetic acid, 1% aniline blue for 8 minutes, then quickly rinsed again with 1% acetic acid, dehydrated in ethanol, and mounted in cyto seal mounting reagent. Bone volume was quantified as previously described (Merrill et al., 2008). To quantify bone in cultured mandibles, histological sections were digitized using a Leica DM 2500 (Leica Microsystems, Inc. Buffalo Grove, IL) with a color digital camera system (SPOT Insight 4 Megapixel CCD, Diagnostic Instruments, Inc., Sterling Heights, MI). NIH

ImageJ/Fiji (Schindelin et al., 2012) was used to count pixels comprising bone matrix. Bone matrix volume (BV) was estimated using the equation for a conical frustum: $BV = (1/3h) ((A_i + A_{ii}) + (\sqrt{A_i A_{ii}}))$; where “h” is distance between sections (7µm), and “A_i” and “A_{ii}” are areas (in µm) of bone in sequential sections (Colnot et al., 2003; Lu et al., 2005). P values were calculated using a Paired Student’s t-test with two tailed distribution.

Gene Expression Analysis Using *In situ* Hybridization

Whole heads from chick embryos at HH24 and HH27 were fixed in 4% PFA and embedded in paraffin and sectioned as described above. 10µm sections were hybridized with digoxigenin (DIG)-labeled antisense riboprobes synthesized from chick cDNA as previously described (Woronowicz et al., 2018). Sections were treated with 10 µg/ml proteinase K for 8 to 25 minutes, hybridized overnight at 65°C with either *Cxcl14* or *Wnt11* DIG-labeled antisense probes, and incubated overnight at 4°C with 1:2000 anti-DIG-Alkaline phosphatase antibody (Roche, 11093274910). Color development reactions were carried out for 2 to 4 days.

Cxcl14 in situ probe primers	Fwd: GAGGACGGGAACACAAGACAG
	Rev: TAATACGACTCACTATAGGGGAGAAATCATCTTC
Wnt11 in situ probe primers	Fwd: TTCTGCAGACGGGGAATTTGC
	Rev: TAATACGACTCACTATAGCGTATCTCT
Cxcl14 qPCR primers	Fwd: CGGAAGGCGTAAAGTGCAAA
	Rev: GTACCACTTCAGCAGCCTCA
Wnt11 qPCR primers	Fwd: AACTACCTGCTGGACTTAGAGAG
	Rev: TGGTGCAGGCTCTGGCAATG

Gene Expression Analysis Using Quantitative PCR

Epithelium, mesenchyme, and whole mandibles of chick HH24, HH27, and cultured mandibles were homogenized using a Bead Mill 24 Homogenizer (Fisher, 15-340-163) at 4m/s for 15 seconds. RNA was extracted using the PicoPure RNA Isolation Kit (ThermoFisher, KIT0204) following the manufacturer's instructions. cDNA was synthesized using 400ng total RNA using iScript cDNA Synthesis Kit (Bio-Rad, 1708841) with the following cycles: 25⁰C for 5 minutes, 42⁰C for 30 minutes, and 85⁰C for 5 minutes. Each quantitative PCR used 5ng of cDNA and was carried out using the iQ SYBR Green Supermix (Bio-Rad, 1708882) following previously published protocols (Dole et al., 2015; Smith et al., 2016). Each biological sample was assayed in technical duplicate. Gene expression levels were normalized against 18S rRNA.

Gain- and Loss-of-Function

Cxcl14 was cloned into the pPIDNB expression vector as described in Chapter 3 (Chu et al., 2020), which generates mRNA bidirectionally and allows independent translation of the mNG protein and cDNA of interest. 3 μ l of a solution including the inducible expression vector pPIDNB (3 μ g/ μ l), the transposase pNano-hyPBase (1 μ g/ μ l), and a small amount of Fast Green dye was loaded into a pulled glass micro-injection needle. For bilateral electroporation, either pPIDNB-Cxcl14 or empty vector (i.e., pPIDNB-GFP) was electroporated into presumptive NCM along the neural tube of chick embryos at HH8-9 using three square pulses at 50 V for 1 ms spaced 50 ms apart in the reverse polarity using the or BEX CUY21EDITII Pulse Generator. For unilateral electroporation, expression vectors were electroporated into presumptive NCM along the right side of the

neural tube of chick embryos at HH8-9 (which allows for an internal control on the contralateral side). We used three square pulses at 50 V for 1 ms spaced 50 ms apart, followed by five square pulses at 10 V for 50 ms spaced 50 ms apart. 1mg/ml doxycycline (Acros organics, 446060250) was diluted in HBSS at the ratio 2.5 μ l:750 μ l and was gently dropped onto the vitelline membrane when the embryo reached HH18. When the mandibles reached HH22, they were cultured in BgJB medium (Thermo, 12591038) supplemented with 10% F10% FBS (VWR, 97068-085, Lot# 283K18), 1X penicillin-streptomycin (Thermo Fisher Scientific, 15140122), and 50 μ g/ml ascorbic acid. For WNT gain- or loss-of-function experiments, WNT activator (BIO) (Stem Cell Technologies, 72034) or WNT inhibitor (IWP2) (Stem Cell Technologies, 72124) was added to the culture media, respectively. Culture media was replaced every two to three days. Ex ovo mandibles were cultured for up to seven days and assayed for bone using trichrome histology staining.

Western Blot

DF-1 cells were harvested in 1X RIPA lysis buffer (EMD Millipore, 20-188) containing Halt protease inhibitors (Thermo Fisher Scientific, 78430). Protein concentration was quantified by BCA assay (Thermo Fisher Scientific, 23225). 40 μ g of protein was loaded per lane of a 15% SDS polyacrylamide gel. Protein transfer was carried out using an Immobilon-PPVDF membrane (Millipore, Billerica, MA, IPVH00010). Membranes were probed with primary antibodies including rabbit anti-CXCL14 (0.2 μ g/ml, Peprotech, 500-P237) and mouse anti-chick β -actin antibody (1:4000, Novus Biologicals, NB600-501), and secondary antibodies including goat anti-rabbit IRDye 800CW (1:15000, LI-COR

#925-32211), and donkey anti-mouse IRDye 680RD antibody (1:15000, LI-COR #925-68072). Fluorescent signal was captured using the Odyssey Imaging System (Thermo Fisher Scientific).

Results

RNA-seq Reveals NCM-Mediated Genes in Mandibular Epithelium

Our previous work has shown that faster-developing quail donor NCM signals to duck host epithelium instructively and accelerates the timing of the EMI required for osteogenesis (Merrill et al., 2008). Thus, the EMI are accelerated in quack such that the requirement for osteoinductive signals from duck host epithelium ends at HH24 instead of HH27, and bone forms prematurely (Merrill et al., 2008). This reveals that osteogenic signals in the mandibular epithelium are regulated by NCM and follow the timetable of the faster-developing quail donor (Merrill et al., 2008). We leveraged this experimentally-induced shift in the timing of epithelial signaling to screen for the differential expression of novel osteoinductive factors using an RNA-seq strategy in chimeric embryos.

Specifically, our strategy allowed comparisons of epithelial genes both among groups (duck HH24 versus duck HH27) and between groups (duck HH24 versus quack HH24) by accounting for the three-stage difference between donor and host cells (Fish and Schneider, 2014; Lwigale and Schneider, 2008; Schneider and Helms, 2003). Applying stringent criteria to our RNA-seq data, we selected for genes with a two-fold change minimum and $p\text{-value} \leq 0.05$. We identified 29 genes encoding proteins secreted into the extracellular matrix (**Figure 11**).

Notably, we observed that several members of the WNT signaling pathway were differentially expressed in our epithelial dataset. In the candidate gene list, we found upregulated (e.g., DKK2) and downregulated (e.g., WNT11, WNT2B) genes that are secreted molecules in WNT pathway. We also observed additional differentially expressed members and targets of the WNT pathway but these were not secreted molecules and instead include transcription factors such as TCF1, TCF2, TCF/LEF, NFIX, DKK2, and FZD4. Both canonical and non-canonical WNT pathways play an important role in intramembranous osteogenesis and jawbone regeneration (Arnsdorf et al., 2009; Dao et al., 2010; Goldstein et al., 2006; Song et al., 2014; Yan et al., 2009; Yu et al., 2005). In this study, I have identified the WNT pathway alongside *Cxcl14* as a potential component of the osteogenic EMI. As such, I tested if the epithelial expression of WNT ligand is mediated by NCM and if altering WNT signaling would affect bone formation.

My results also reveal that the chemokine CXCL14 is expressed at the right time and place during EMI, which is a novel finding for my study. Though its involvement in development is poorly understood, CXCL14 has been shown to interact with BMP and WNT pathways in the context of connective tissue development in the chick limb (Nassari et al., 2017) and embryogenesis in *Xenopus* (Park et al., 2009). Chemokines are a family of proteins originally identified for their activity in attracting key inflammatory immune cells. Recent evidence indicates that chemokines also regulate key developmental processes. In this study, I set out to characterize CXCL14 further and to test its possible role in bone formation in the lower jaw.

Validation of Candidate Genes

Further investigation using RT-qPCR and section *in situ* hybridization (ISH) validated that expression of *Cxcl14*, *Wnt11* and *Wnt2b* (data not shown) significantly change in epithelium during EMI ($p < 0.01$; Figure 12). At HH24, *Cxcl14* expression is relatively low whereas *Wnt11* expression is detected in mandibular epithelium. However, at HH27, *Cxcl14* expression in mandibular epithelium increases about 2-fold compared to HH24 ($p < 0.0005$) and *Wnt11* expression decreases by about 2-fold ($p < 0.0005$).

Because previous studies have shown that osteogenic signals in the epithelium are regulated by NCM (Fish and Schneider, 2010; Merrill et al., 2008; Schneider and Eames, 2004), we tested if *Cxcl14* and *Wnt11* expression in mandibular epithelium is also regulated by NCM. To study the effects of NCM on mandibular epithelium, we generated quail-duck chimeras (**Figure 1A**). Taking advantage of differences in embryonic maturation rates, we transplanted NCM from faster-developing Japanese quail into slower-developing White Pekin duck. Osteogenic mesenchyme in the mandible is derived entirely from NCM (Noden, 1978; Noden and Schneider, 2006), and in quack, the faster-developing quail donor NCM interacts with duck host epithelium, which causes differential regulation of various osteogenic genes and accelerates the timing of bone formation (Eames and Schneider, 2008; Hall et al., 2014; Schneider and Helms, 2003). Using qPCR, we assayed for changes in *Cxcl14* and *Wnt11* expression levels in quack epithelium extracted from HH24. Compared to HH24, *Cxcl14* expression in HH24 quack epithelium is upregulated about 3-fold ($p < 0.0001$) and *Wnt11* expression is downregulated by about 2-

fold ($p < 0.05$) compared to its expression at HH24. This confirms that *Cxcl14* and *Wnt11* are indeed regulated by NCM.

In situ hybridization on coronal sections of Chick HH24 mandibles revealed that *Cxcl14* is expressed in very specific domains in the mandible during EMI. Specifically, *Cxcl14* transcripts are found in the distal part (towards the midline) of the mandible in the epithelium and in the proximal part (towards the sides) of the mandible in the mesenchyme. Prior work has shown that *Cxcl14* is expressed in the mandible in distinct nonoverlapping domains of mesenchyme and epithelium such that non-*Cxcl14* expressing epithelium overlays *Cxcl14* expressing mesenchyme and vice versa (Gordon et al., 2011). In contrast, transcripts of *Wnt11* are distributed throughout mandibular mesenchyme in a nonspecific manner at HH21 and become more restricted during HH24-HH29. Interestingly, *Wnt11* is enriched in the distal portion of the mandibular epithelium and mesenchyme where *Cxcl14* is (**Figure 12C + 12D, 12E + 12F, 12G + 12H**). This co-expression pattern suggests a possible interaction between the WNT pathway and *Cxcl14* around HH24-29.

Cxcl14 Overexpression Induces Bone Formation

To study the role of *Cxcl14* during EMI, we used two approaches to overexpress *Cxcl14* in chick mandible *ex ovo* and *in ovo*. The first approach employs pEPIC-*Cxcl14* to overexpress *Cxcl14 ex ovo* (Chu et al., 2020). Chick mandibular primordia were isolated from HH23 embryos, dissected into two halves at the midline and electroporated with either an overexpression construct that carries constitutively active GFP or an empty

construct as a contralateral internal control. After five days of culture, each half was collected and screened for GFP before being fixed for histology. Osteoid staining shows that after five days, the halves with pEPIC-*Cxcl14* have premature mesenchymal condensation and early osteoid staining (n = 3/5) compared to the control halves (n = 0/5) (**Figure 13**). When the organ culture period was extended to seven days, more osteoid staining was found on the treated halves (p = 0.05, paired-t test) (**Figure 14,15**).

In the second approach, chick *Cxcl14* was cloned into the pPIDNB inducible overexpression vector that carries mNeonGreen and mScarlet reporter genes as previously described (Chu et al., 2020). mNeonGreen expression is constitutively active, whereas mScarlet expression only activates upon exposure to doxycycline (dox). The vector was injected into the neural tube of chick embryos at HH8-9 and the tissues were electroporated unilaterally into presumptive NCM on the right side. We first detect mNeonGreen signals along the neural tube about 4 hours post electroporation. At 12 hours post-electroporation, streams of emigrating NCM with mNeonGreen signals were apparent (**Figure 16A**). Once migrating NCM from the first arch arrive at the maxilla and mandible and develop to HH22 (2 days post-electroporation), dox (50ng/ml) was added *in ovo* to induce expression of *Cxcl14*. mScarlet was first detected 2 hours post-induction and became intense within the next 10 hours (**Figure 16B**). Detection of mScarlet confirmed that the constructs were successfully introduced into mandible and integrated into the genome. RT-qPCR results showed that the level of exogenous *Cxcl14* gene expression were significantly higher on the target right site compared to the control left site of the mandible (**Figure 17**). Similarly, Western blot results showed that CXCL14

protein expression is induced in DF-1 cells transfected with *Cxcl14*-FLAG-pPIDNB whereas no CXCL14 protein is detected in control DF-1 cells transfected with empty vector (**Figure 17**).

To test if *Cxcl14* plays a role in regulating any other major tissue during development of the mandibular primordia, I used RT-qPCR to assay for markers of cartilage, nerve, muscle, tendon, and/or bone formation in mandibles with *Cxcl14* overexpression. *Sox9* was used as a lineage marker for cartilage (Bi et al., 1999), *Tnc* for nerve (Reinhard et al., 2017), *MyoD* for muscle (Chal and Pourquie, 2017), *Scx* for tendon (Sakabe et al., 2018), and *Runx2*, *Alp*, and *Col1a* for bone (Stein et al., 2004; Zernik et al., 1990). Compared to control mandibles that were electroporated with empty vectors, overexpressing *Cxcl14* had no effect on expression of *Sox9*, *Tnc*, *MyoD*, or *Scx*, indicating that *Cxcl14* does not regulate the development of cartilage, nerve, muscle, and tendon lineages during mandibular morphogenesis. In contrast, expression levels for markers of osteogenesis (i.e., *Runx2*, *Alp*, and *Col1a*) were significantly induced following the overexpression of *Cxcl14*, suggesting that *Cxcl14* is osteoinductive (**Figure 18**).

To test if *Cxcl14* can induce and/or augment the formation of bone, mandibles were electroporated with *Cxcl14*-pPIDNB, harvested at HH23, cultured for seven days, collected, and sectioned. For each electroporated mandible, the left side contained *Cxcl14* overexpressing NCM whereas the right side was devoid of signal, which served as a contralateral internal control. Compared to the control side, the side with *Cxcl14* over-expression had more osteoid (**Figure 19A, B**). mScarlet signal overlapped with

osteoid-positive areas, indicating that *Cxcl14* overexpression induces premature intramembranous ossification (**Figure 19C, C'**). mScarlet signal was also found in areas surrounding cartilage where periosteum bone was forming (**Figure 19D, D'**). By quantifying the volume of osteoid I confirmed that *Cxcl14* over-expression significantly enhances mandibular osteogenesis on the experimental side compared to the internal control side after seven days of culture (n=10, p<0.05) (**Figure 20**).

WNT Signaling Positively Regulates Mandibular Osteogenesis

Although WNT signaling is known to promote osteogenesis, the role of WNT signaling during the EMI required for mandibular osteogenesis is not known. Our RNA-seq experiment revealed that members and targets of the WNT signaling pathway are differentially expressed during the EMI required for mandibular osteogenesis, suggesting WNTs may be important. To test if WNT signaling affects mandibular osteogenesis during EMI, we manipulated the WNT pathway in cultured mandibles using a WNT activator (i.e., BIO) and a WNT inhibitor (i.e., IWP2). BIO (6-bromoindirubin-3'-oxime) acts as a WNT activator by inhibiting the WNT-inhibiting GSK3 α protein, thus activating the canonical WNT signaling pathway (Sato et al., 2004). IWP2 acts as a WNT inhibitor by inhibiting Porcupine, which is important for the palmitoylation and subsequent secretion of WNT proteins, thus inhibiting both noncanonical and canonical WNT signaling pathways (Chen et al., 2009).

Mandibles were isolated from chick embryos HH22, treated at successive concentrations with either the WNT activator (i.e., 1 μ M, 5 μ M, 10 μ M, and 20 μ M) or the WNT inhibitor

(i.e., 1, 5 and 50 μM), cultured for seven days, fixed, and sectioned. Control mandibles were cultured in DMSO. Compared to control mandible treated with DMSO that formed normal osteoid after seven days of culture (**Figure 21A**), mandibles cultured with the WNT activator displayed altered osteoid formation (**Figure 21B, B'**). In contrast, bone formation in mandibles cultured with the WNT inhibitor was negatively impacted. We found that increasing the concentration of IWP2 (i.e., 1 μM , 5 μM and 30 μM) increases the inhibition of mandibular osteogenesis. At 50 μM of IWP2, osteogenesis is completely blocked (**Figure 21C**).

Quantification of osteoid volume demonstrates that at increasing concentrations of the WNT activator, more bone formation is found, especially at 10 μM BIO ($p < 0.05$). Interestingly, at a higher concentration (BIO = 20 μM), less bone forms (**Figure 22**). One explanation for this is that at too high a concentration, BIO over activates WNT signaling and subsequently has a negative effect on bone formation. In contrast, inhibiting WNT signaling using IWP2 correlates with less bone forming in the lower jaw primordia. At 50 μM IWP2, sufficient WNT signaling was inhibited such that no bone formation was found even after seven days of culture (**Figure 21B**).

The WNT Pathway Regulates CXCL14

Because data from sectioned RNA in situ indicates transcripts of *Cxcl14* and *Wnt11* are found in overlapping domains in the lower jaw primordia, we wanted to test if there was an interaction between WNT signaling and *Cxcl14*. Chicken mandibles at HH23 were cut in half and one half was cultured *ex ovo* with either the WNT activator BIO (10 μM) or

WNT inhibitor IWP2 (5 μ M). The other contralateral half was cultured in DMSO as an internal control. After one and two days of culture, the samples were collected and assayed for expression of *Cxcl14* using RT-qPCR. The results showed that *Cxcl14* expression was consistently higher in the side treated with WNT activator BIO after both one and two days of culture (n = 6 per group, p<0.05) compared to the control sides. In contrast, *Cxcl14* expression was always lower on the side treated with WNT inhibitor IWP2 compared to the control side in all cases (n = 6 per group, p<0.05) (**Figure 23**). This suggests that *Cxcl14* expression is regulated by the WNT pathway. Specifically, WNT signaling may play a role in inducing *Cxcl14* in mandibular epithelium.

To study if this potential crosstalk between WNTs and *Cxcl14* affects osteogenesis, we performed a WNT inhibitor rescue experiment. Because we found that the WNT inhibitor disrupts bone formation in the mandible at a high enough concentration, we tested if overexpressing *Cxcl14* would be able to rescue osteogenesis in mandibles treated with the WNT inhibitor. Chick embryos were electroporated at HH8-9 with the *Cxcl14*-pPIDNB vector. Mandibles from these embryos were screened for positive mNeonGreen signals and collected at HH22-23. These samples were cultured for seven days in BGJb media with the WNT inhibitor (30 μ M) and with either DMSO (control samples, n = 10) or Doxycycline (50 ng/ml, tested samples, n = 26) to induce *Cxcl14* expression. Media was changed every two to three days and after seven days of culture, the samples were collected. Trichrome staining on sectioned samples showed that in control samples, WNT inhibitor IWP2 consistently blocked osteoid formation in all cases (n = 10). Strikingly, overexpressing *Cxcl14* was able to rescue bone formation in the mandible even when

WNT signaling is inhibited (n = 11/26) (**Figure 21E**). The areas forming osteoid tended to be small islands close to cartilage and containing *Cxcl14*-overexpressing cells as confirmed by positive mScarlet signal.

Discussion

We designed an RNA-seq experiment (**Figure 1**) to identify NCM-dependent genes that were differentially expressed in duck host mandibular epithelium of chimeric quack due to the presence of faster-developing donor quail NCM. Our strategy was successful, and we identified many genes that potentially could play a role. For this study, we focused on *Wnt11* and *Cxcl14*. Multiple lines of evidence suggested that both these genes may work in tandem to regulate the EMI underlying mandibular osteogenesis. This evidence includes overlapping expression domains and rescue experiments. Previous studies have shown that *Wnt11* plays a role in osteoblast differentiation in vivo (Ealba et al., 2015; Wang et al., 2016) but the role of WNT signaling during mandibular EMI has not been explored. In addition, the role of *Cxcl14* during jaw skeleton development has not been elucidated, yet its spatiotemporal expression pattern is tantalizingly specific to the region where mandibular bone eventually forms, suggesting a novel role for *Cxcl14*.

It takes five to six days for chick mesenchymal cells harvested at HH23 to start making osteoid. We wanted to see if over-expressing *Cxcl14* could affect the timing and amount of osteoid formation. Our experiments demonstrate that overexpressing *Cxcl14* leads to premature mesenchymal condensation and the initiation of osteogenesis within five days of mandible culture. Moreover, overexpressing *Cxcl14* and allowing the cultures to grow

for up to seven days increases the amount of osteoid. To test if increasing *Cxcl14* expression can promote more bone formation during later stages, we electroporated quail embryos with pPIDNB-*Cxcl14* at HH8.5, induced *Cxcl14* expression with dox, and collected the embryos at HH37. While many of these embryos display no obvious skeletal phenotype (n = 28), some specimens (n = 2) display an abnormally longer lower jaw (**Figure 24**). There are several possibilities to explain this observed phenotype. First, *Cxcl14* over-expression in enough cells may drive early osteogenesis and accelerate bone formation, thus giving the treated sample a “head start”; although there may be some unidentified checkpoints in place at later stages of development that inhibit the overgrowth of bone such that we only observe abnormal bone growth in 7% (2/28 samples) of cases. Secondly, only those samples with *Cxcl14* overexpressed at the right place would manifest a skeletal phenotype. CXCL14 is a small molecule secreted into the extracellular matrix, yet how far CXCL14 can diffuse is unknown. If CXCL14 only acts over a short range, then having CXCL14 protein made in the right local area to induce osteoblast differentiation is critical.

Though several members of WNT pathway are differentially expressed in mandibular epithelia according to our RNA seq dataset, our study focused on *Wnt11* and the effect WNT signaling has on osteogenesis. As *Wnt11* has been reported to belong to both canonical and noncanonical pathways, we decided to use a chemical approach to target the entire pathway. The WNT activator BIO specifically activates the canonical WNT-signaling by inhibiting the downstream WNT inhibitor GSK3 α and allows activation of β -catenin. The WNT inhibitor IWP2 actually blocks both canonical and noncanonical WNT

pathways by inhibiting secretion of WNT ligands. Our data indicate that WNT signaling is required for osteogenesis, since blocking WNT pathway by IWP2 inhibits bone formation, while increasing WNT signaling by BIO promotes bone formation. Whether bone formation is promoted at the expense of cartilage under the influence of activating WNT signaling is not clear, and more work needs to be done to parse out the effects on different lineages. However, we also observed that WNT inhibitor IWP2 not only reduces bone formation but also increases cartilage formation, although quantification of the effect of IWP2 on Meckel's cartilage remains to be investigated.

Upregulated and downregulated genes identified by the RNA-seq experiment do not simply correlate with promoting and inhibiting bone formation. In fact, although WNT signaling is downregulated at HH27 compared to HH24, and *Cxcl14* is upregulated, our experiments show that activating WNT signaling and over-expressing *Cxcl14* both promote bone formation. The downregulation of WNT ligands in the epithelium during EMI corresponds to the timing of when the mesenchyme no longer requires epithelium to form bone. This change in spatial expression is also similar to that observed for *Bmp4*. *Bmp4* is downregulated at HH27 as its expression transitions from epithelium to mesenchyme, and adding exogenous BMP4 actually promotes bone formation in the mandibular primordia (Merrill et al., 2008). *Wnt11* likely acts in a similar manner where its expression goes down in the epithelium during EMI as its domain of expression becomes restricted to the distal parts of the mesenchyme, as evidenced by our *in situ* hybridization. Furthermore, WNT signaling and *Cxcl14* appear to act in the same axis where WNT is upstream and regulates CXCL14, which explains why activating WNT and/or CXCL14

induces bone formation. Notably, *Cxcl14* expression seems more sensitive to IWP2 than to BIO (**Figure 23**), suggesting that *Cxcl14* is likely regulated by both canonical and non-canonical WNT pathways.

Our published work shows that *Bmp4* can promote mandibular bone formation when epithelium remains intact yet cannot substitute for the epithelium in inducing bone formation (Merrill et al., 2008). Importantly, there is some evidence that BMP and WNT pathways are involved in regulating CXCs in ectoderm (Park et al., 2009) and bone fracture healing (Myers et al., 2015). Therefore, we tested if activating WNT and *Cxcl14* individually and in combination with *Bmp4* promote mandibular osteogenesis in the absence of epithelium during the stage when mesenchyme still depends on epithelium. We found that these combination treatments are not sufficient to recapitulate osteogenic epithelial signaling as no osteoid forms during the period when NCM still relies on epithelium to make bone. This indicates other additional factors are probably required in conjunction with *Bmp4* to replace mandibular epithelium to induce bone formation.

In summary, we have utilized an *in vivo* genetic approach in combination with *ex ovo* organ culture to address the question whether NCM-mediated differentially expressed genes in the epithelium can alter osteogenesis in mandibular primordia. Our results suggest that WNT signaling and *Cxcl14* interact and promote osteogenesis, likely in parallel with BMP signaling. This project is significant for investigating epithelial factors regulated by NCM that were initially identified in a relatively normal *in vivo* context. Consequently, our results have the potential to be highly relevant for creating new

strategies to treat craniofacial defects. More research remains to be done to uncover additional secreted factors by the epithelium as they can play a major role in allowing NCM to differentiate to osteoblasts.

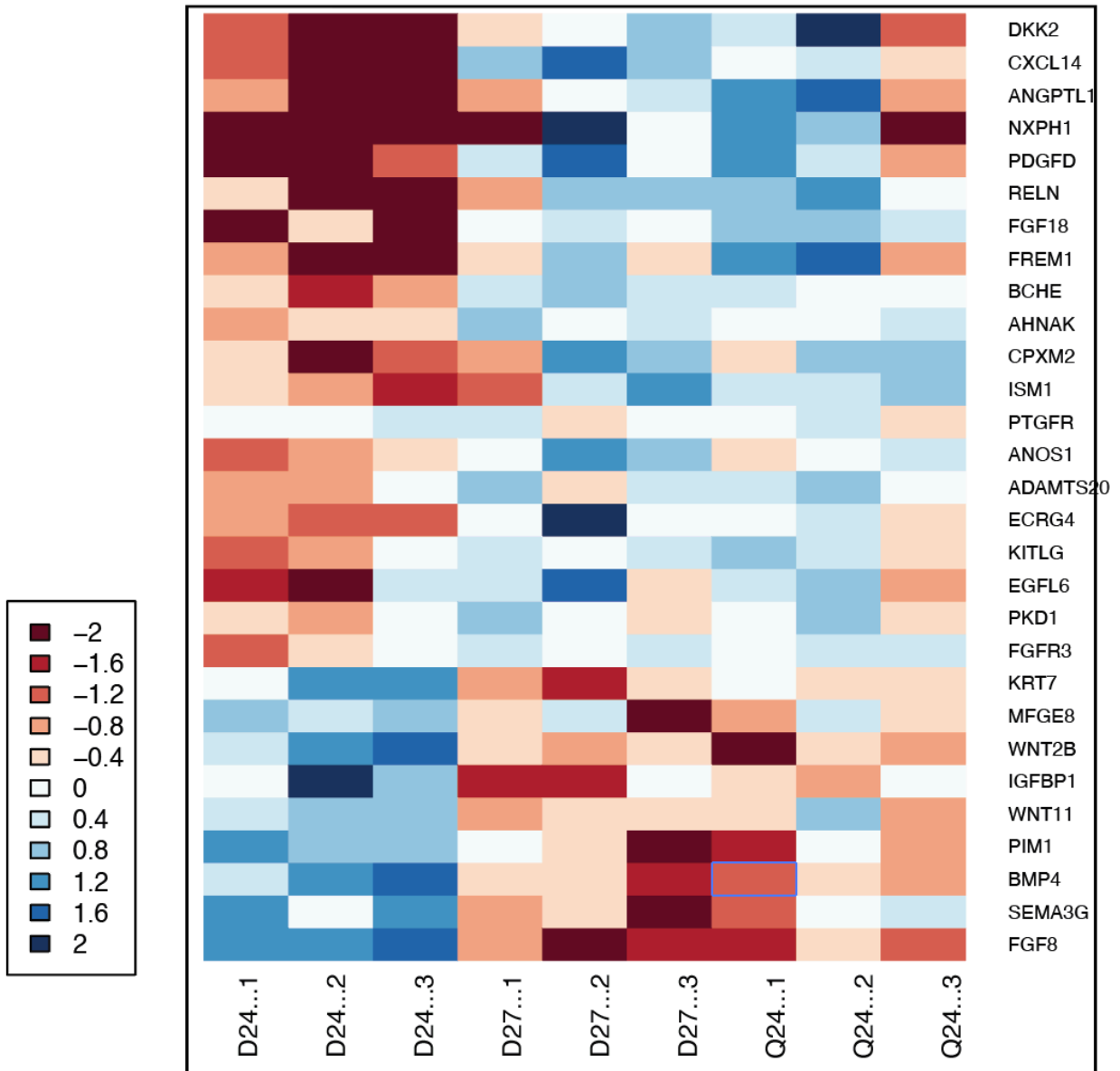


Figure 4.2: Heat map analysis of genes differentially expressed in Duck HH24 vs Duck HH27 and Duck HH24 vs Quack HH24.

Upregulated genes are on top of the table, downregulated genes are at the bottom of the table.

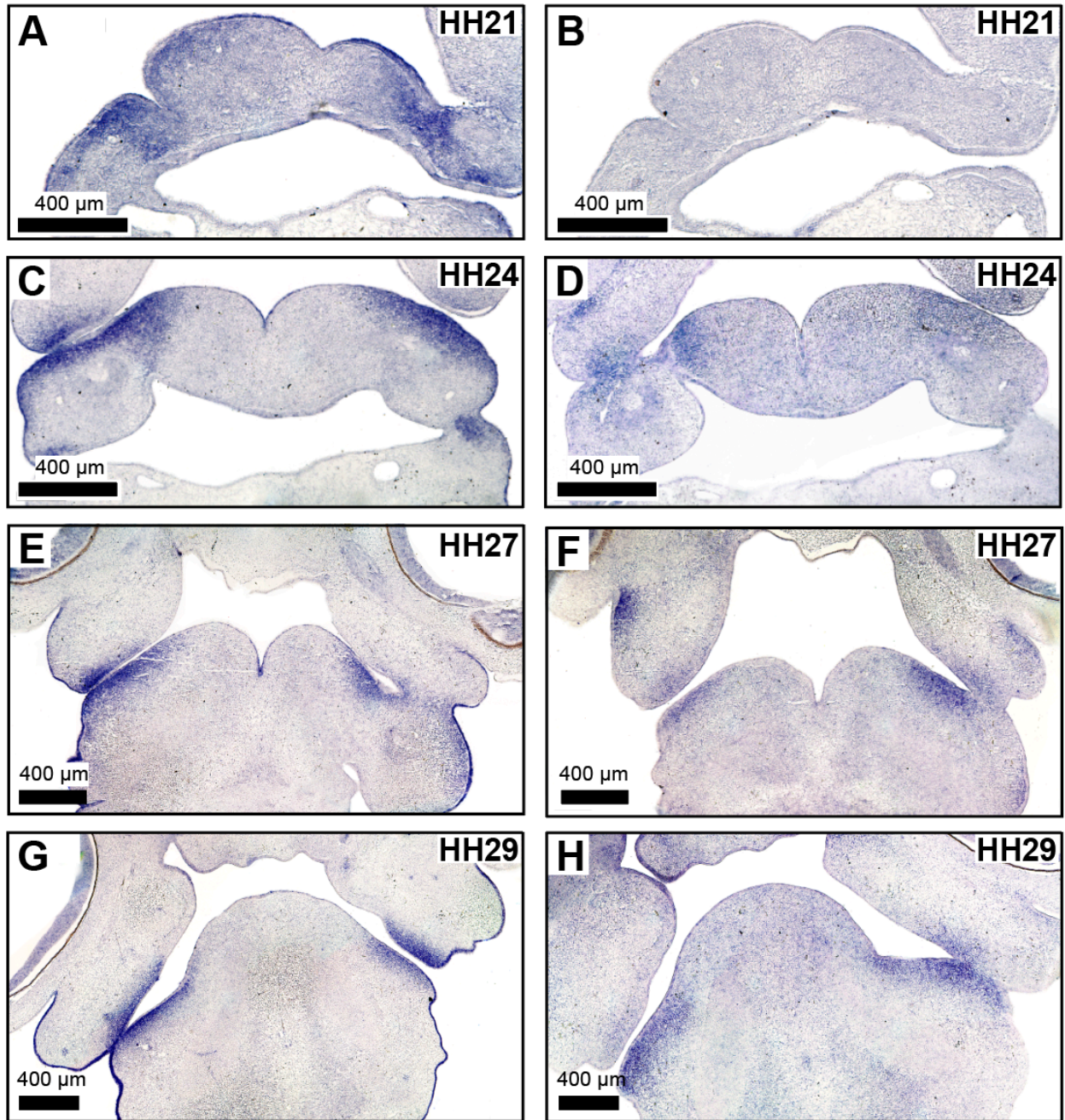


Figure 4.3: *Cxcl14* and *Wnt11* expression in Chick mandibular primordia.

Cxcl14 (left column) and *Wnt11* (right column) RNA in situ hybridization on adjacent coronal sections of Chick HH21, HH24, HH27, and HH29 mandibles.

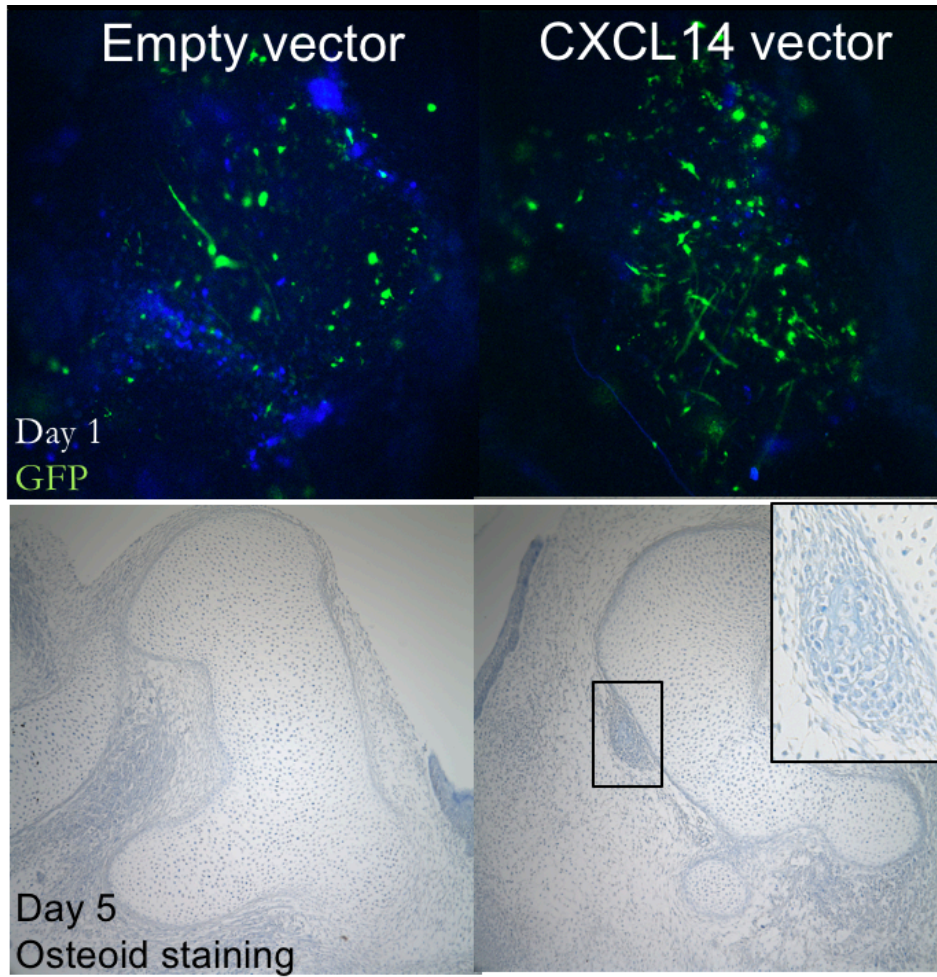


Figure 4.4: *Cxcl14* overexpression and early mesenchymal condensation.

Chick HH23 mandibles overexpressing *Cxcl14* have premature mesenchymal condensation and early osteoid staining (n=3/5 with osteoid staining) compared to control (n=0/5 with osteoid staining) after 5 days of culture.

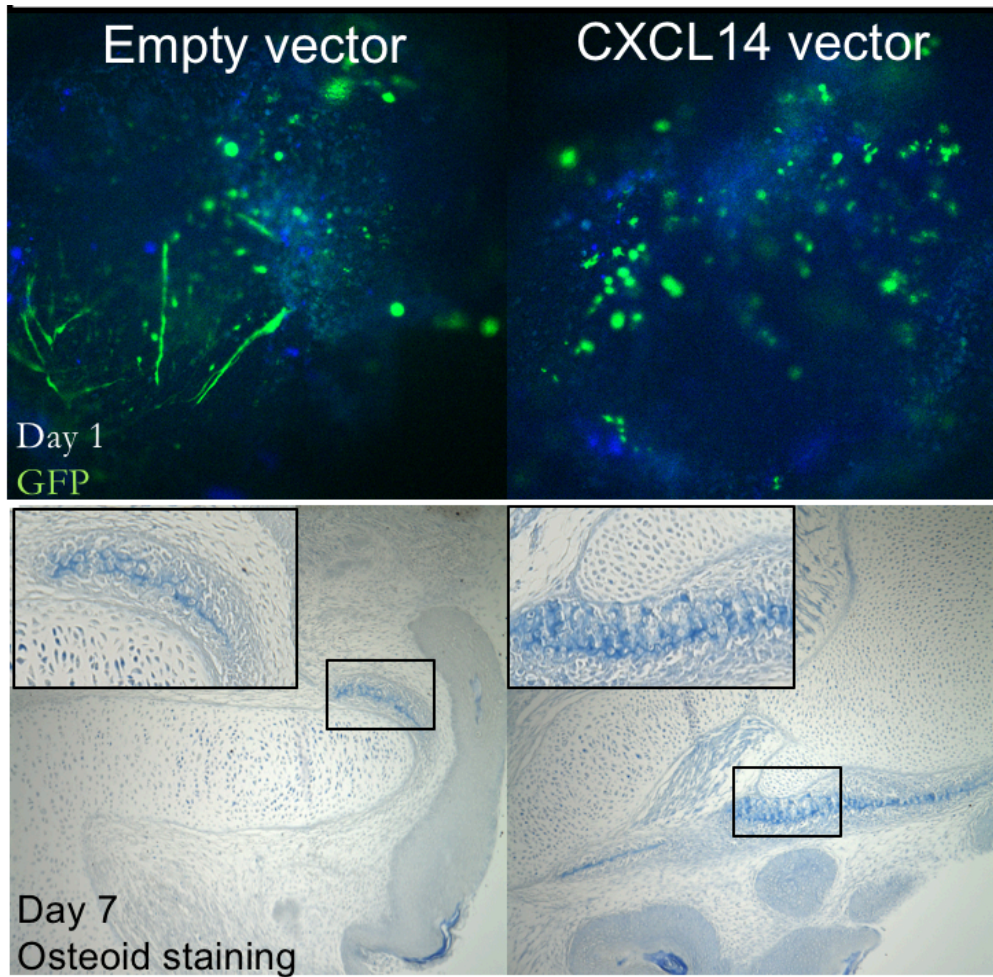


Figure 4.5: *Cxcl14* overexpression and early bone formation.

Chick HH23 mandibles overexpressing *Cxcl14* have more osteoid staining compared to control after 7 days of culture.

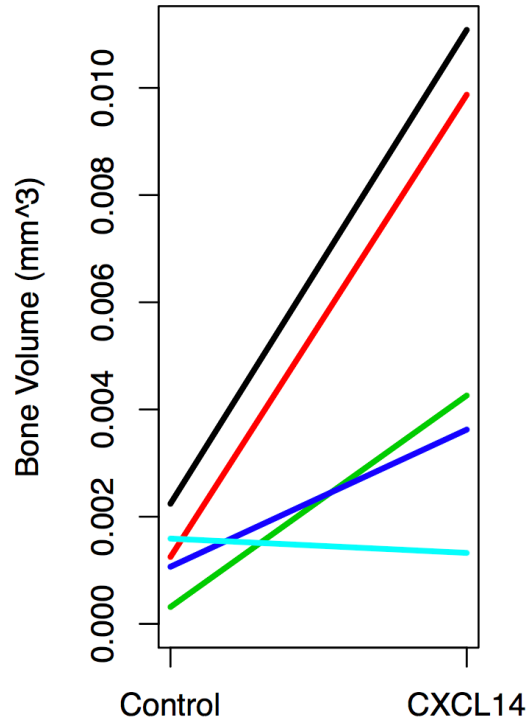


Figure 4.6: Quantification of bone formation in mandibles overexpressing *Cxcl14* vs controls.

Mandibular sides overexpressed with *Cxcl14* display more bone formation compared to the contralateral control side ($p=0.05$, paired t-test).

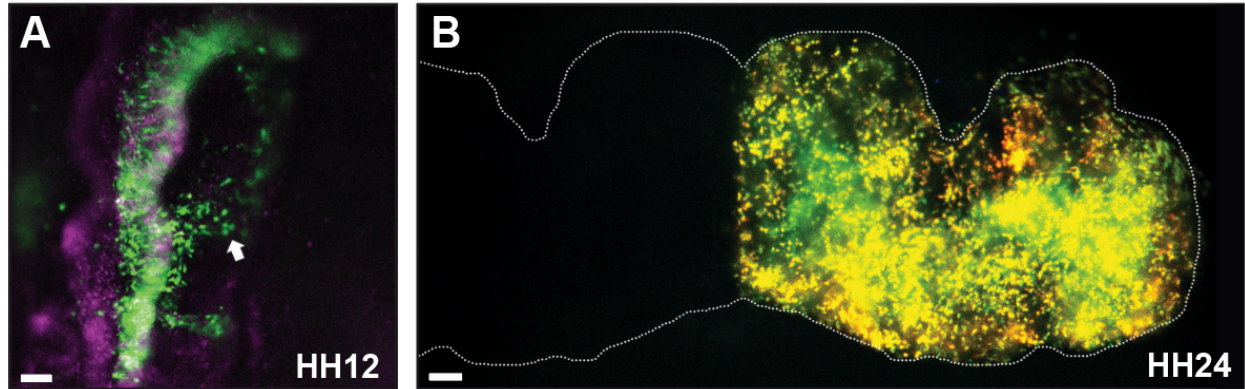


Figure 4.7: In vivo induction of *Cxcl14* in chick mandibular primordia.

pPIDNB carrying *Cxcl14* was unilaterally electroporated into HH8.5 neural crest cells along the neural tube at the level of the 1st and second pharyngeal arches. (A) 12 hours post electroporation when embryo reaches stage HH12, in ovo imaging shows robust mNeonGreen signals. mNeonGreen acts as a constitutively active reporter gene that indicates cells that incorporated the plasmids with overexpressed *Cxcl14*. Neural crest cells that migrate into the first pharyngeal arch (arrow) differentiate into neural crest mesenchymal cells that give rise to osteoblasts. (B) Two days post electroporation when embryo reaches stage HH22, dox is added to induce expression of *Cxcl14*. mScarlet reporter gene turns on upon induced, indicating the location of CXCL14 overexpression. Lower jaw primordia at HH24 reveals fluorescent signals only present on the right side while the left side serves as an internal control.

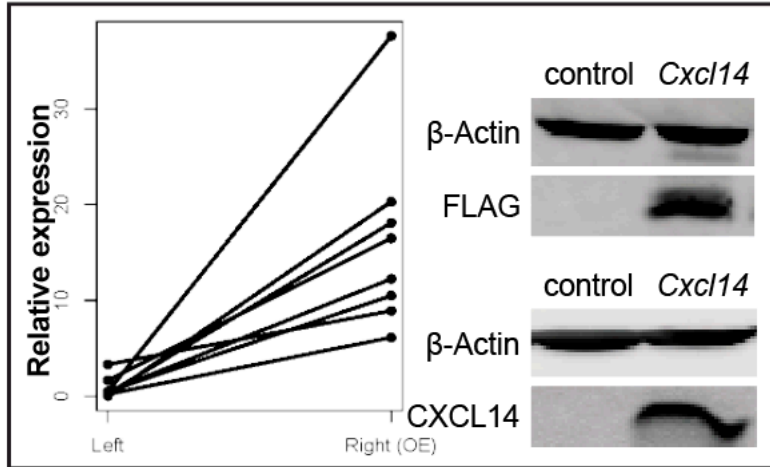


Figure 4.8: Verification of overexpression level of *Cxcl14*.

RT-qPCR confirmed that the right side with *Cxcl14* overexpression (OE) has higher levels of exogenous expression of *Cxcl14* compared to the left internal control side within the same mandible ($p < 0.05$, students paired t-test). Western blot confirmed that DF1 cells overexpressed with either CXCL14 with a FLAG tag or CXCL14 both make proteins with the appropriate molecular weight for CXCL14 (14kDa).

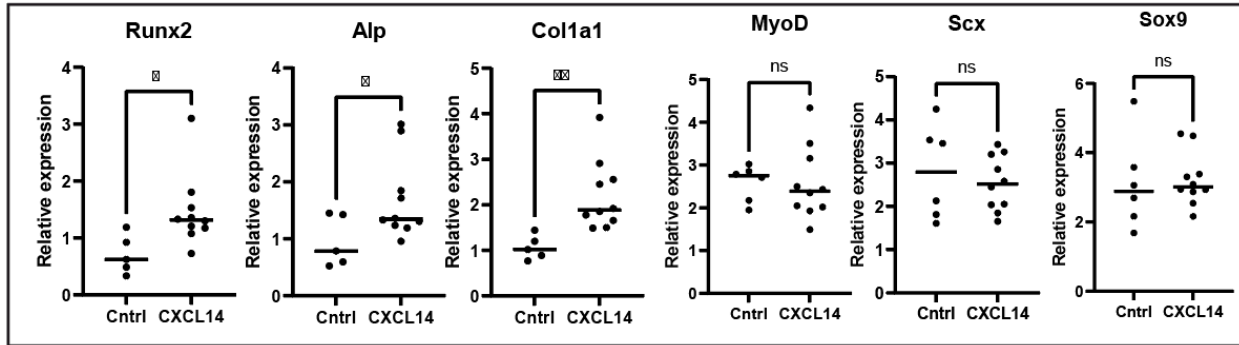


Figure 4.9: The role of *Cxcl14* in regulating bone formation.

Cxcl14 OE samples display higher levels of expression of bone lineage markers. Different connective tissue markers are used to assess if *Cxcl14* OE can induce different cell lineage differentiation. RT-qPCR results show that *Cxcl14* OE is specific in induce bone markers (Runx2, Alp, and Col1a, $p < 0.05$), but does not alter expression of other lineages, including muscle (MyoD), tendon (Scx), cartilage (Sox9).

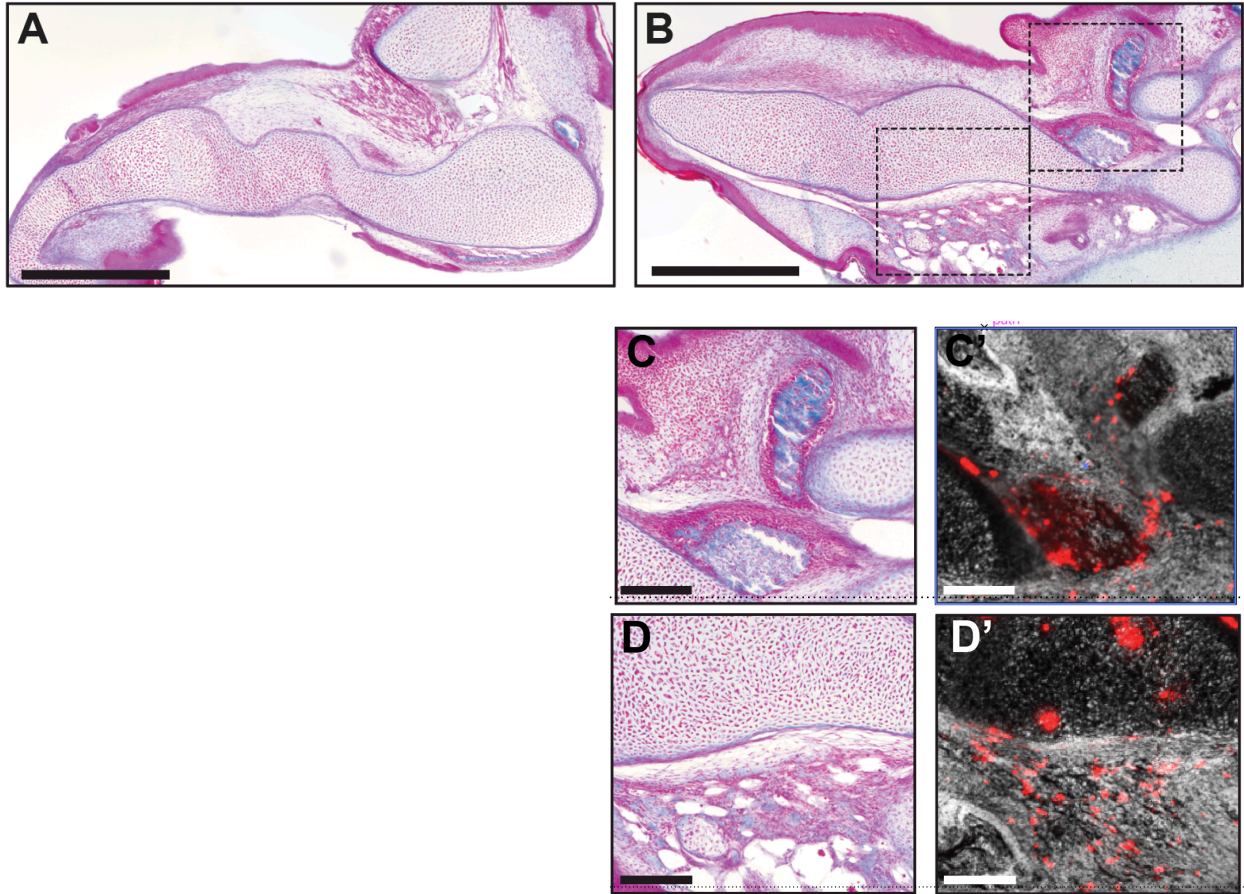


Figure 4.10: The role of *Cxcl14* in regulating bone formation.

Trichrome staining of Left (control) side (A) vs Right (*Cxcl14* OE) side (B) after seven days of culture show more bone formation on the right side. mScarlet signal are found in areas where membranous bone (C, C') and periosteum bone (D, D') form.

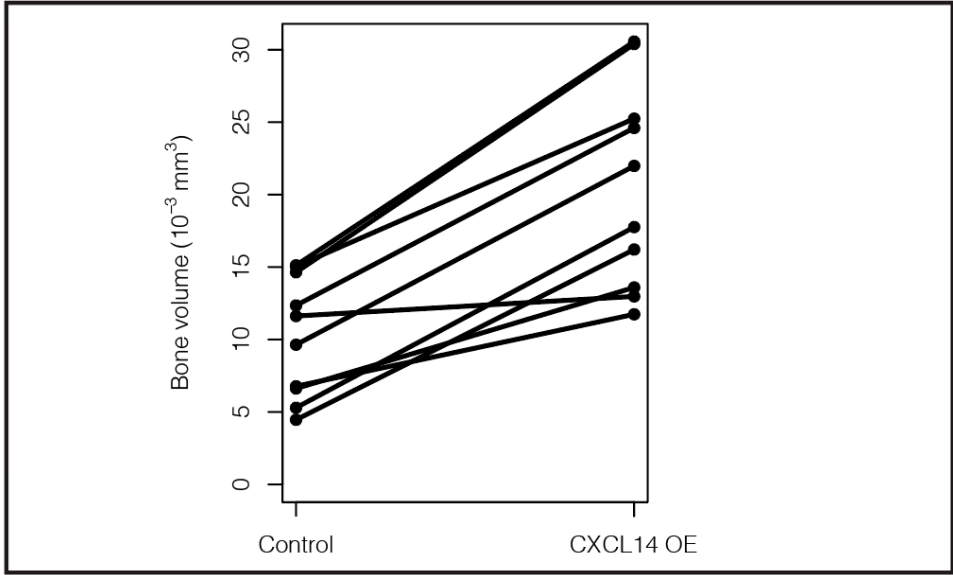


Figure 4.11: Quantification of bone formation in *Cxcl14* OE sides vs control sides.

Quantification of osteoid volume on the left (control) side vs right (*Cxcl14* OE) side shows *Cxcl14* OE is correlated with more osteoid volume ($p < 0.05$).

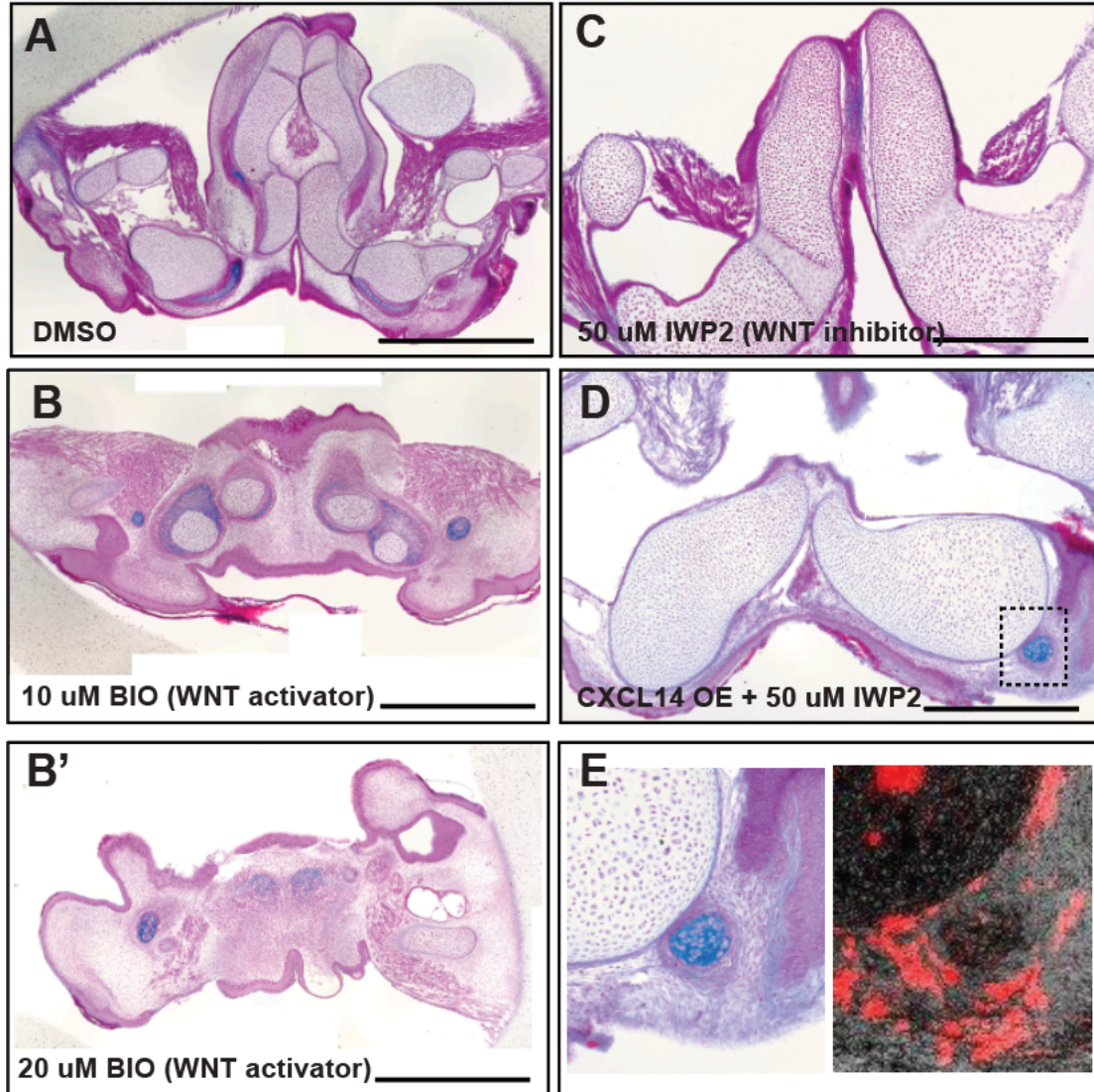


Figure 4.12: Altering WNT signaling and the resulting phenotypes.

Trichrome staining of mandibles cultured with DMSO (A), WNT activator BIO (B, B'), and WNT inhibitor IWP2 (C) show modulating WNT signaling alters osteogenesis in mandible. At 50 μ M, WNT inhibitor IWP2 completely blocks bone formation (C), but overexpressing *Cxcl14* can induce bone formation despite the presence of IWP2 (D). Bone forming areas overlap with mScarlet signals (E).

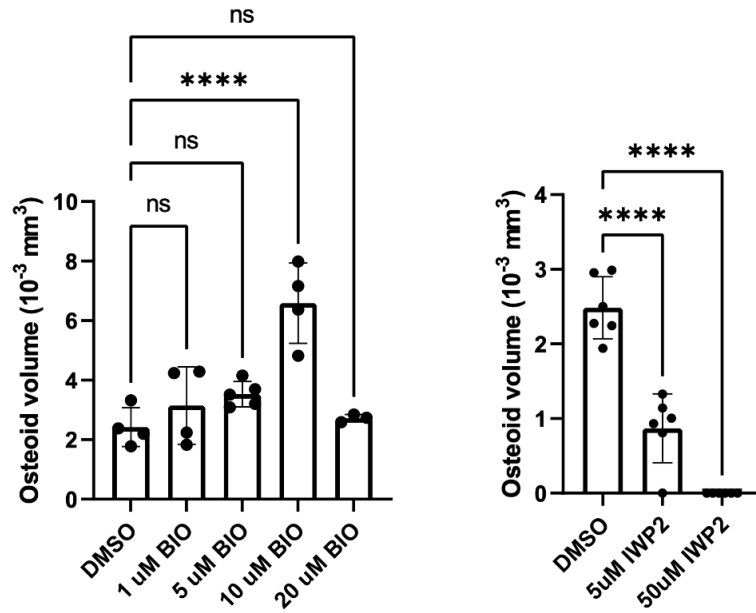


Figure 4.13: Quantification of bone formation resulting from activating and inhibiting WNT signaling.

WNT signaling affects bone formation in lower jaw primordia. Chick HH22 mandibles were cultured in DMSO (control), or WNT activator at increasing concentrations (1, 5, 10, 20 μM of BIO), or WNT inhibitor at increasing concentrations (5, 50 μM of IWP2) for seven days then sectioned for osteoid volume quantification.

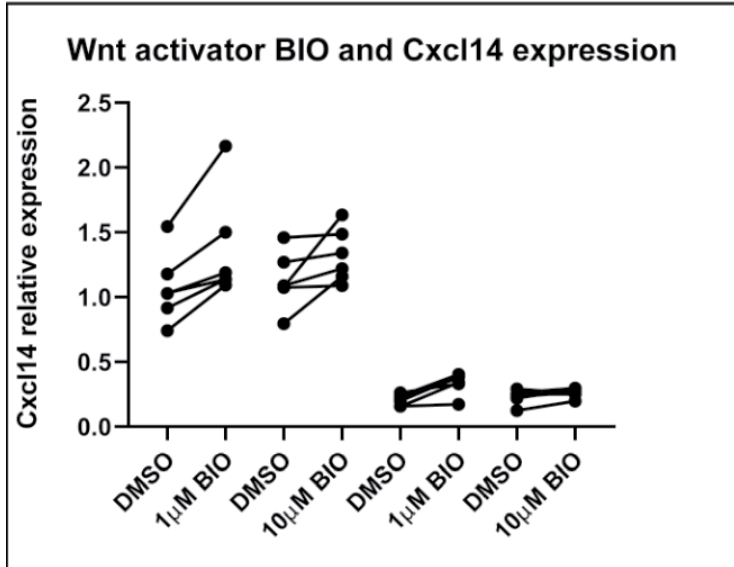
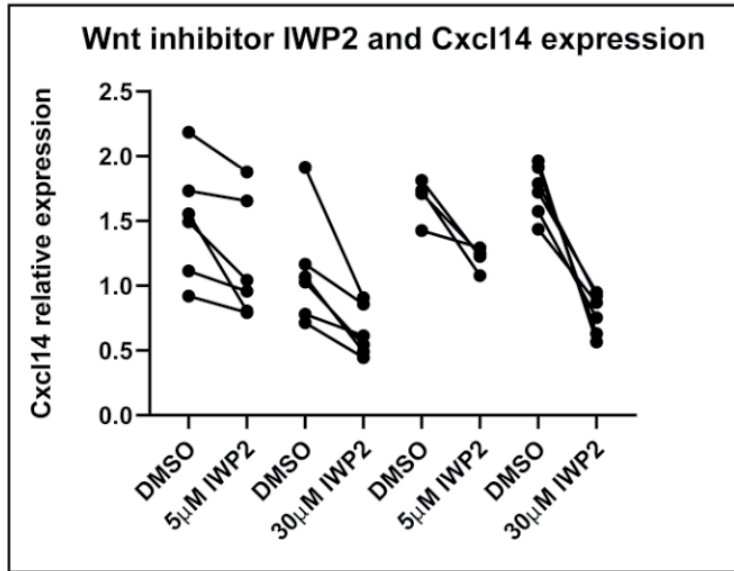


Figure 4.14: WNT signaling as an upstream regulator of *Cxcl14*.

WNT signaling regulates *Cxcl14* expression. HH23 Chick mandibles were dissected in halves at midline and treated with WNT inhibitor or WNT activator at different concentrations while the other counterpart side treated with DMSO as control. Organ cultures were maintained for one and two days then collected and assayed for expression levels of *Cxcl14* ($p < 0.05$, paired t-test).

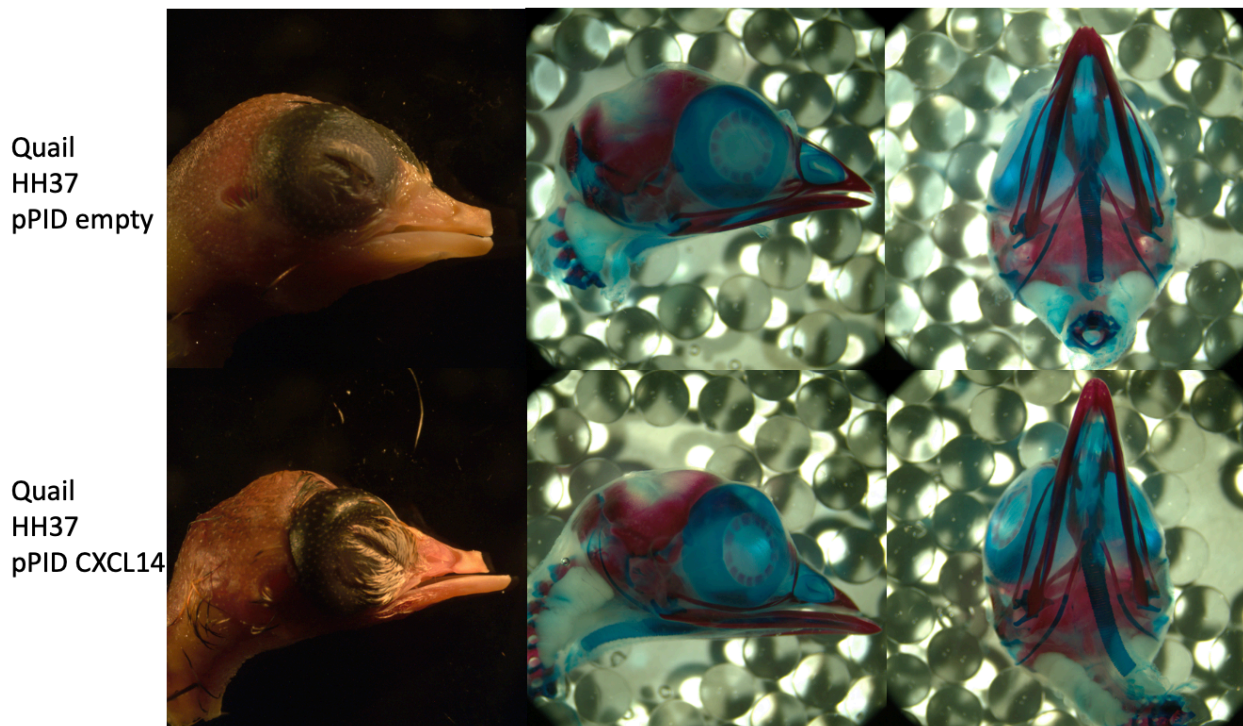


Figure 4.15: Abnormally longer lower jaw found in quail overexpressing *Cxcl14*.

Quail pPID-*Cxcl14* OE HH37 display a longer lower jaw phenotype (n=2/28). Quail neural crest cells destined to migrate to the presumptive mandibular primordia were electroporated with either pPID empty vector as a control (top panel) or pPID-*Cxcl14* (bottom panel) at HH8.5 bilaterally, collected at HH37, and fixed in 4% PFA (first column) then cleared and stained with Alcian blue and Alizarin red to identify cartilage and bone, respectively. Side (second column) and inferior (third column) views.

Chapter 5: Summary and Future Directions

With the goal of devising new molecular-based therapies for diseases, birth defects, and injuries to the jaw skeleton, I have endeavored to identify mechanisms that promote the formation of bone. Previous studies have shown that EMI are required for mandibular mesenchyme to form bone (Bradamante and Hall, 1980; Dunlop and Hall, 1995; Hall, 1978; Hall and Coffin-Collins, 1990; Hall and Van Exan, 1982; Helms and Schneider, 2003; Merrill et al., 2008; Sharpe and Ferguson, 1988; Tyler and Hall, 1977; Tyler and McCobb, 1980; Van Exan and Hall, 1984; Wedden, 1987). Such interactions likely result in the epithelium secreting osteoinductive factors many of which remain unidentified. Discovering these factors could have significant clinical applications for regenerating bone.

Published work from our lab and others using avian embryos has revealed that mandibular mesenchyme cannot form bone when grown in culture without overlying epithelium at HH24, but can starting around HH27 (Hall, 1978; Merrill et al., 2008; Tyler and McCobb, 1980). Thus, mesenchyme depends upon epithelial signals until HH27. Previously, we identified and showed that one of these epithelial signals, Bone Morphogenetic Protein 4 (BMP4), can augment bone formation when delivered to mandibles in culture (Merrill et al., 2008). However, we found that BMP4 alone is insufficient to promote osteogenesis in mesenchyme cultured without adjacent epithelium (Merrill et al., 2008). Thus, additional epithelial signals are needed. In this study, we identified a novel role for two potential epithelial factors, *Cxcl14* and *Wnt11*, which we demonstrated are involved in mandibular osteogenesis. These genes have an osteogenic effect during EMI, yet combining CXCL14 and WNT signaling with BMP4 was not able to

recapitulate the totality of epithelial signaling. This suggests that other factors may be required to enable mesenchyme to act independent of the epithelium. Some of these other factors are likely hidden in plain sight among the list of genes identified by our RNA-seq results. Future work will continue to explore this list and experiment with various combinations of activating and inhibitory signals with the goal of making more bone. Specifically, we plan to investigate other secreted factors identified as differentially expressed genes from the RNA-seq data. Members of WNT signaling, including WNT2b, FZD4, and DKK2 are high on the list and can easily be cloned into our over-expression system that we developed and electroporated into HH8.5 embryos. This gain-of-function approach can quickly screen for genes of interest that effect osteogenesis.

Because overexpressing *Cxcl14* generated more bone during early osteogenesis, we wanted to test if knocking down *Cxcl14* would affect jaw skeletogenesis. To do so, we used an RCAS CXCL14shRNA construct that was a gift from Dr. P Lwigale. Although RCAS-shRNA successfully knocks down *Cxcl14* and RCAS-CXCL14 increases *Cxcl14* expression in vitro (**Figure 25**), RCAS retroviral vectors do not appear to change *Cxcl14* expression in vivo (data not shown). We are planning future experiments to overcome this technical difficulty with reducing CXCL14 expression, including designing morpholinos and developing a CRISPRi system to be used in avians.

Additionally, we are very much interested in transcriptional regulation of *Cxcl14* especially by members and targets of the WNT signaling pathway. With this in mind, we have begun to perform a *Cxcl14* promoter mapping analysis *in silico*, and have identified potential

binding sites for various transcription factors 2 kb upstream of the transcription start site for *Cxcl14*. This analysis will likely shed light on specific upstream mechanisms that regulate *Cxcl14* and elucidate its ability to induce bone. Thus far, we have found several transcription factor binding elements for known members of the WNT signaling pathway as well as for transcription factors that interact with WNT signaling, including NFIX (Wu et al., 2021), NFIA (Hasenpusch-Theil et al., 2012), MEIS3 (Elkouby et al., 2010), TBX4 (Takeuchi et al., 2003), and DLX3 (Sun et al., 2019). NFIX has been reported to induce osteoblast differentiation (Wu et al., 2021). MEOX2 mutation has been found in bone healing defects, and craniofacial and skeletal abnormalities (Kim et al., 2020; Tran et al., 2018). PDX1 is associated with osteogenic differentiation of adipose derived stem cells via the PI3K/Akt pathway (Liu et al., 2022). Loss of TBX4 is found in abnormal development of lower limbs and pelvis in humans (Bongers et al., 2004). The DLX transcription factor family appears to interact with *Cxcl14* promoter as well. DLX2 and DLX3 overexpression can promote osteogenesis *in vitro* (Sun et al., 2019; Zhang et al., 2019), while DLX4, DLX5, and DLX6 are associated with defects in cleft palate, bone formation, and other jaw anomalies (Robledo et al., 2002; Samee et al., 2008; Wu et al., 2015, Samee, 2008 #4271). To validate these transcription factors, we can start with luciferase assays as our lab has done previously (Smith et al., 2022).

In the context of promoting bone healing, recombinant BMPs are being used (Henderson et al., 2016; Kanakaris et al., 2008) but their controversial efficacy begs for alternative molecular choices (Boden et al., 2002; Kim and Valentini, 2002; Miyamoto and Takaoka, 1993). In the future, activating CXCL14 and WNT signaling and studying their roles in

promoting healing of bone fractures and regeneration of osteoblasts in a mouse model could also be tested. Interestingly, IWP2, the WNT inhibitor, displays a striking phenotype that appears to completely block bone formation, presumably pushing mesenchymal cells towards chondrogenesis. Clinical cases that require cartilage regeneration could take advantage of this finding. Overall, my research project has advanced our understanding of mechanisms underlying EMI in the mandible and I am optimistic that such studies may lead to potentially novel therapeutic approaches to promote bone formation in the jaw following birth defects, disease, or injury.

Materials and Methods

RCAS-CXCL14shRNA virus production and *in vivo* injection

The avian retroviral vectors were obtained from the lab of Dr. P. Lwigale. RCAS(B)-*Cxcl14*shRNA was designed to carry either one of 4 sequences targeting *Cxcl14* mRNA at 170, 210, 268, and 308 base position from the starting sequence of chick CXCL14 mRNA. RCAS(A)-CXCL14 carries a 296-bp cDNA fragment containing the coding region of chick *Cxcl14*. DF1 cells grown to 70% confluence were transfected with 1 μ g of RCAS plasmid using Lipofectamine following manufacturer's protocol (Sigma). Virus-containing supernatants were collected when at least 95% of the cells were infected by RCAS virus, assayed by GFP expression and 3C2 antibody staining. Viral particles were concentrated by ultracentrifugation at 4⁰C for 1.5hr at 21,000rpm. High titer virus was injected into cranial region of HH8 chick embryos which were collected at HH37 and processed for skeletal prep.

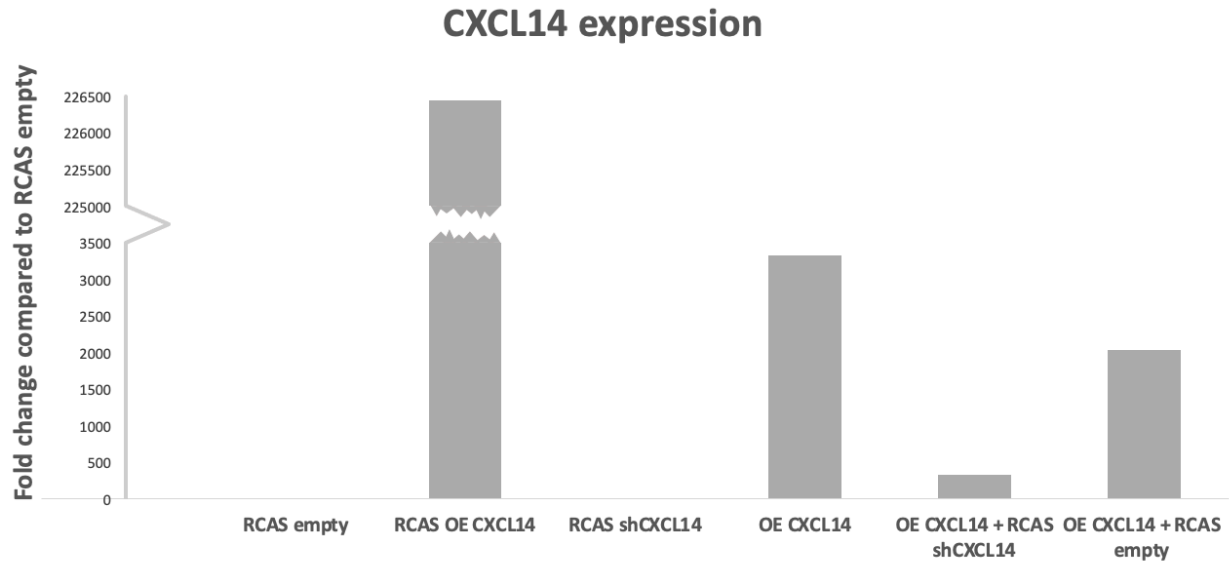


Figure 5.1: *Cxcl14* loss-of-function experiment using RCAS-shRNA.

RT-qPCR shows RCAS-CXCL14 and RCAS-CXCL14shRNA are transfected to DF1 cells and target *Cxcl14* specifically.

References

Aaboe, M., Pinholt, E.M., Hjrting-Hansen, E., 1995. Healing of experimentally created defects: a review. *British Journal of Oral and Maxillofacial Surgery* 33, 312-318.

Ahler, E., Sullivan, W.J., Cass, A., Braas, D., York, A.G., Bensinger, S.J., Graeber, T.G., Christofk, H.R., 2013. Doxycycline alters metabolism and proliferation of human cell lines. *PLoS One* 8, e64561.

Ainsworth, S.J., Stanley, R.L., Evans, D.J., 2010. Developmental stages of the Japanese quail. *J Anat* 216, 3-15.

Albrektsson, T., Johansson, C., 2001. Osteoinduction, osteoconduction and osseointegration. *Eur Spine J* 10 Suppl 2, S96-101.

Alexander-Savino, C.V., Hayden, M.S., Richardson, C., Zhao, J., Poligone, B., 2016. Doxycycline is an NF-kappaB inhibitor that induces apoptotic cell death in malignant T-cells. *Oncotarget* 7, 75954-75967.

Arnsdorf, E.J., Tummala, P., Kwon, R.Y., Jacobs, C.R., 2009. Mechanically induced osteogenic differentiation--the role of RhoA, ROCKII and cytoskeletal dynamics. *J Cell Sci* 122, 546-553.

Bahrami, F., Morris, D.L., Pourgholami, M.H., 2012. Tetracyclines: drugs with huge therapeutic potential. *Mini Rev Med Chem* 12, 44-52.

Balk, M.L., Bray, J., Day, C., Epperly, M., Greenberger, J., Evans, C.H., Niyibizi, C., 1997. Effect of rhBMP-2 on the osteogenic potential of bone marrow stromal cells from an osteogenesis imperfecta mouse (oim). *Bone* 21, 7-15.

Bi, W., Deng, J.M., Zhang, Z., Behringer, R.R., de Crombrughe, B., 1999. Sox9 is required for cartilage formation. *Nat Genet* 22, 85-89.

Boden, S.D., Kang, J., Sandhu, H., Heller, J.G., 2002. Use of recombinant human bone morphogenetic protein-2 to achieve posterolateral lumbar spine fusion in humans: a prospective, randomized clinical pilot trial: 2002 Volvo Award in clinical studies. *Spine (Phila Pa 1976)* 27, 2662-2673.

Bongers, E.M., Duijf, P.H., van Beersum, S.E., Schoots, J., Van Kampen, A., Burckhardt, A., Hamel, B.C., Losan, F., Hoefsloot, L.H., Yntema, H.G., Knoers, N.V., van Bokhoven, H., 2004. Mutations in the human TBX4 gene cause small patella syndrome. *Am J Hum Genet* 74, 1239-1248.

Bradamante, Z., Hall, B.K., 1980. The role of epithelial collagen and proteoglycan in the initiation of osteogenesis by avian neural crest cells. *Anatomical Record* 197, 305-315.

Chal, J., Pourquie, O., 2017. Making muscle: skeletal myogenesis in vivo and in vitro. *Development* 144, 2104-2122.

Chen, B., Dodge, M.E., Tang, W., Lu, J., Ma, Z., Fan, C.W., Wei, S., Hao, W., Kilgore, J., Williams, N.S., Roth, M.G., Amatruda, J.F., Chen, C., Lum, L., 2009. Small molecule-mediated disruption of Wnt-dependent signaling in tissue regeneration and cancer. *Nat Chem Biol* 5, 100-107.

Chu, D., Nguyen, A., Smith, S.S., Vavrusova, Z., Schneider, R.A., 2020. Stable integration of an optimized inducible promoter system enables spatiotemporal control of gene expression throughout avian development. *Biology Open* 9.

Collins, P.J., McCully, M.L., Martinez-Munoz, L., Santiago, C., Wheeldon, J., Caucheteux, S., Thelen, S., Cecchinato, V., Laufer, J.M., Purvanov, V., Monneau, Y.R., Lortat-Jacob, H., Legler, D.F., Uguccioni, M., Thelen, M., Piguet, V., Mellado, M., Moser, B., 2017. Epithelial chemokine CXCL14 synergizes with CXCL12 via allosteric modulation of CXCR4. *FASEB J* 31, 3084-3097.

Colnot, C., Z.Thompson, Miclau, T., Werb, Z., Helms, J.A., 2003. Altered fracture repair in the absence of MMP9. *Development* in press.

Cong, L., Ran, F.A., Cox, D., Lin, S., Barretto, R., Habib, N., Hsu, P.D., Wu, X., Jiang, W., Marraffini, L.A., Zhang, F., 2013. Multiplex genome engineering using CRISPR/Cas systems. *Science* 339, 819-823.

Dann, C.E., Hsieh, J.C., Rattner, A., Sharma, D., Nathans, J., Leahy, D.J., 2001. Insights into Wnt binding and signalling from the structures of two Frizzled cysteine-rich domains. *Nature* 412, 86-90.

Dao, D.Y., Yang, X., Flick, L.M., Chen, D., Hilton, M.J., O'Keefe, R.J., 2010. Axin2 regulates chondrocyte maturation and axial skeletal development. *J Orthop Res* 28, 89-95.

de Boer, H.H., 1988. The history of bone grafts. *Clin Orthop Relat Res*, 292-298.

Dixon, J., Jones, N.C., Sandell, L.L., Jayasinghe, S.M., Crane, J., Rey, J.P., Dixon, M.J., Trainor, P.A., 2006. Tcof1/Treacle is required for neural crest cell formation and proliferation deficiencies that cause craniofacial abnormalities. *Proc Natl Acad Sci U S A* 103, 13403-13408.

Dole, N.S., Kapinas, K., Kessler, C.B., Yee, S.P., Adams, D.J., Pereira, R.C., Delany, A.M., 2015. A single nucleotide polymorphism in osteonectin 3' untranslated region regulates bone volume and is targeted by miR-433. *J Bone Miner Res* 30, 723-732.

Dunlop, L.L., Hall, B.K., 1995. Relationships between cellular condensation, preosteoblast formation and epithelial-mesenchymal interactions in initiation of osteogenesis. *International Journal of Developmental Biology* 39, 357-371.

Ealba, E.L., Jheon, A.H., Hall, J., Curantz, C., Butcher, K.D., Schneider, R.A., 2015. Neural crest-mediated bone resorption is a determinant of species-specific jaw length. *Dev Biol* 408, 151-163.

Ealba, E.L., Schneider, R.A., 2013. A simple PCR-based strategy for estimating species-specific contributions in chimeras and xenografts. *Development* 140, 3062-3068.

Eames, B.F., Schneider, R.A., 2005. Quail-duck chimeras reveal spatiotemporal plasticity in molecular and histogenic programs of cranial feather development. *Development* 132, 1499-1509.

Eames, B.F., Schneider, R.A., 2008. The genesis of cartilage size and shape during development and evolution. *Development* 135, 3947-3958.

Elkouby, Y.M., Elias, S., Casey, E.S., Blythe, S.A., Tsabar, N., Klein, P.S., Root, H., Liu, K.J., Frank, D., 2010. Mesodermal Wnt signaling organizes the neural plate via Meis3. *Development* 137, 1531-1541.

Ermak, G., Cancasci, V.J., Davies, K.J., 2003. Cytotoxic effect of doxycycline and its implications for tet-on gene expression systems. *Anal Biochem* 318, 152-154.

Fish, J.L., Schneider, R.A., 2010. The role of neural crest progenitor population specification and proliferation dynamics in establishing species-specific differences in jaw size. *Develop Biol* 344, 419.

Fish, J.L., Schneider, R.A., 2014. Assessing species-specific contributions to craniofacial development using quail-duck chimeras. *J Vis Exp* 87, 1-6.

Francis-West, P., Ladher, R., Barlow, A., Graveson, A., 1998. Signalling interactions during facial development. *Mechanisms of Development* 75, 3-28.

Gandhi, S., Piacentino, M.L., Vieceli, F.M., Bronner, M.E., 2017. Optimization of CRISPR/Cas9 genome editing for loss-of-function in the early chick embryo. *Dev Biol* 432, 86-97.

Garrison, K.R., Shemilt, I., Donell, S., Ryder, J.J., Mugford, M., Harvey, I., Song, F., Alt, V., 2010. Bone morphogenetic protein (BMP) for fracture healing in adults. *Cochrane Database Syst Rev* 2010, CD006950.

Goldstein, B., Takeshita, H., Mizumoto, K., Sawa, H., 2006. Wnt signals can function as positional cues in establishing cell polarity. *Developmental cell* 10, 391-396.

Gordon, C.T., Wade, C., Brinas, I., Farlie, P.G., 2011. CXCL14 expression during chick embryonic development. *Int J Dev Biol* 55, 335-340.

Gorlin, R.J., Cohen, M.M., Levin, L.S., 1990. *Syndromes of the Head and Neck*, 3rd ed. Oxford University Press, New York.

Hall, B.K., 1978. Initiation of osteogenesis by mandibular mesenchyme of the embryonic chick in response to mandibular and non-mandibular epithelia. *Archives of Oral Biology* 23, 1157-1161.

Hall, B.K., 1980. Tissue interactions and the initiation of osteogenesis and chondrogenesis in the neural crest-derived mandibular skeleton of the embryonic mouse as seen in isolated murine tissues and in recombinations of murine and avian tissues. *Journal of Embryology and Experimental Morphology* 58, 251-264.

Hall, B.K., 1981. The induction of neural crest-derived cartilage and bone by embryonic epithelia: an analysis of the mode of action of an epithelial-mesenchymal interaction. *Journal of Embryology and Experimental Morphology* 64, 305-320.

Hall, B.K., 1982. Distribution of osteo- and chondrogenic neural crest-derived cells and of osteogenically inductive epithelia in mandibular arches of embryonic chicks. *Journal of Embryology and Experimental Morphology* 68, 127-136.

Hall, B.K., 1988. The Embryonic Development of Bone, *American Scientist*, pp. 174-181.

Hall, B.K., 2000. Epithelial-mesenchymal interactions. *Methods Mol Biol* 137, 235-243.

Hall, B.K., Coffin-Collins, P.A., 1990. Reciprocal interactions between epithelium, mesenchyme, and epidermal growth factor (EGF) in the regulation of mandibular mitotic activity in the embryonic chick. *Journal of Craniofacial Genetics and Developmental Biology* 10, 241-261.

Hall, B.K., Miyake, T., 1992. The membranous skeleton: the role of cell condensations in vertebrate skeletogenesis. *Anat Embryol (Berl)* 186, 107-124.

Hall, B.K., Van Exan, R.J., 1982. Induction of bone by epithelial cell products. *Journal of Embryology and Experimental Morphology* 69, 37-46.

Hall, B.K., Van Exan, R.J., Brunt, S.L., 1983. Retention of epithelial basal lamina allows isolated mandibular mesenchyme to form bone. *Journal of Craniofacial Genetics and Developmental Biology* 3, 253-267.

Hall, J., Jheon, A.H., Ealba, E.L., Eames, B.F., Butcher, K.D., Mak, S.S., Ladher, R., Alliston, T., Schneider, R.A., 2014. Evolution of a developmental mechanism: Species-specific regulation of the cell cycle and the timing of events during craniofacial osteogenesis. *Dev Biol* 385, 380-395.

Hamburger, V., Hamilton, H.L., 1951. A series of normal stages in the development of the chick embryo. *Journal of Morphology* 88, 49-92.

Hamilton, H.L., 1965. *Lillie's development of the Chick. An Introduction to Embryology.* Holt, Rinehart and Winston, New York.

Hampel, G.A., Yilmaz, E., Massrey, C., Clifton, W., Iwanaga, J., Loukas, M., Tubbs, R.S., 2022. History of Bone Grafts in Spine Surgery. *Cureus* 14, e24655.

Hara, T., Nakayama, Y., 2009. CXCL14 and insulin action. *Vitam Horm* 80, 107-123.

Hara, T., Tanegashima, K., 2014. CXCL14 antagonizes the CXCL12-CXCR4 signaling axis. *Biomol Concepts* 5, 167-173.

Hasenpusch-Theil, K., Magnani, D., Amaniti, E.M., Han, L., Armstrong, D., Theil, T., 2012. Transcriptional analysis of Gli3 mutants identifies Wnt target genes in the developing hippocampus. *Cereb Cortex* 22, 2878-2893.

Haxaire, C., Haÿ, E., Geoffroy, V., 2016. Runx2 Controls Bone Resorption through the Down-Regulation of the Wnt Pathway in Osteoblasts. *Am J Pathol* 186, 1598-1609.

Helms, J.A., Schneider, R.A., 2003. Cranial skeletal biology. *Nature* 423, 326-331.

Henderson, D.J., Rushbrook, J.L., Stewart, T.D., Harwood, P.J., 2016. What Are the Biomechanical Effects of Half-pin and Fine-wire Configurations on Fracture Site Movement in Circular Frames? *Clin Orthop Relat Res* 474, 1041-1049.

Holm, S., 1979. A simple sequentially rejective multiple test procedure. *Scandinavian journal of statistics*, 65-70.

Ito, Y., Yeo, J.Y., Chytil, A., Han, J., Bringas, P., Jr., Nakajima, A., Shuler, C.F., Moses, H.L., Chai, Y., 2003. Conditional inactivation of *Tgfr2* in cranial neural crest causes cleft palate and calvaria defects. *Development* 130, 5269-5280.

James, A.W., LaChaud, G., Shen, J., Asatrian, G., Nguyen, V., Zhang, X., Ting, K., Soo, C., 2016. A Review of the Clinical Side Effects of Bone Morphogenetic Protein-2. *Tissue Eng Part B Rev* 22, 284-297.

Jenzer, A.C., Schlam, M., 2022. Retrognathia, StatPearls, Treasure Island (FL).

Jheon, A.H., Schneider, R.A., 2009. The cells that fill the bill: neural crest and the evolution of craniofacial development. *J Dent Res* 88, 12-21.

Jiang, Z., Von den Hoff, J.W., Torensma, R., Meng, L., Bian, Z., 2014. Wnt16 is involved in intramembranous ossification and suppresses osteoblast differentiation through the Wnt/beta-catenin pathway. *J Cell Physiol* 229, 384-392.

Jones, N.C., Lynn, M.L., Gaudenz, K., Sakai, D., Aoto, K., Rey, J.P., Glynn, E.F., Ellington, L., Du, C., Dixon, J., Dixon, M.J., Trainor, P.A., 2008. Prevention of the neurocristopathy Treacher Collins syndrome through inhibition of p53 function. *Nat Med* 14, 125-133.

Jumper, J., Evans, R., Pritzel, A., Green, T., Figurnov, M., Ronneberger, O., Tunyasuvunakool, K., Bates, R., Zidek, A., Potapenko, A., Bridgland, A., Meyer, C., Kohl, S.A.A., Ballard, A.J., Cowie, A., Romera-Paredes, B., Nikolov, S., Jain, R., Adler, J., Back, T., Petersen, S., Reiman, D., Clancy, E., Zielinski, M., Steinegger, M., Pacholska, M., Berghammer, T., Bodenstein, S., Silver, D., Vinyals, O., Senior, A.W., Kavukcuoglu, K., Kohli, P., Hassabis, D., 2021. Highly accurate protein structure prediction with AlphaFold. *Nature* 596, 583-589.

Kanakaris, N.K., Calori, G.M., Verdonk, R., Burssens, P., De Biase, P., Capanna, R., Vangosa, L.B., Cherubino, P., Baldo, F., Ristiniemi, J., Kontakis, G., Giannoudis, P.V., 2008. Application of BMP-7 to tibial non-unions: a 3-year multicenter experience. *Injury* 39 Suppl 2, S83-90.

Kim, H.D., Valentini, R.F., 2002. Retention and activity of BMP-2 in hyaluronic acid-based scaffolds in vitro. *J Biomed Mater Res* 59, 573-584.

Kim, T.Y., Park, J.K., Prasad Aryal, Y., Lee, E.S., Neupane, S., Sung, S., Pokharel, E., Yeon, C.Y., Kim, J.Y., Jung, J.K., Yamamoto, H., An, C.H., Lee, Y., Sohn, W.J., Jang, I.H., An, S.Y., Kim, J.Y., 2020. Facilitation of Bone Healing Processes Based on the Developmental Function of Meox2 in Tooth Loss Lesion. *Int J Mol Sci* 21.

Kloen, P., Doty, S.B., Gordon, E., Rubel, I.F., Goumans, M.J., Helfet, D.L., 2002. Expression and activation of the BMP-signaling components in human fracture nonunions. *J Bone Joint Surg Am* 84-A, 1909-1918.

Kumar, A., Mohamed, E., Tong, S., Chen, K., Mukherjee, J., Lim, Y., Wong, C.M., Boosalis, Z., Shai, A., Pieper, R.O., Gupta, N., Perry, A., Bollen, A.W., Molinaro, A.M., Solomon, D.A., Shieh, J.T.C., Phillips, J.J., 2022. CXCL14 Promotes a Robust Brain Tumor-Associated Immune Response in Glioma. *Clin Cancer Res* 28, 2898-2910.

Leary, S., Underwood, W., Anthony, R., Cartner, S., Corey, D., Grandin, T., Greenacre, C., Gwaltney-Brant, S., McCrackin, M.A., Meye, R., Miller, D., Shearer, J., Yanong, R., Golab, G.C., Patterson-Kane, E., 2013. *AVMA Guidelines for the Euthanasia of Animals: 2013 Edition*, American Veterinary Medical Association, Schaumburg, IL.

Leucht, P., Kim, J.B., Helms, J.A., 2008. Beta-catenin-dependent Wnt signaling in mandibular bone regeneration. *J Bone Joint Surg Am* 90 Suppl 1, 3-8.

Li, G., Bouxsein, M.L., Luppen, C., Li, X.J., Wood, M., Seeherman, H.J., Wozney, J.M., Simpson, H., 2002. Bone consolidation is enhanced by rhBMP-2 in a rabbit model of distraction osteogenesis. *J Orthop Res* 20, 779-788.

Liu, F., Chen, G.D., Fan, L.K., 2022. Knockdown of PDX1 enhances the osteogenic differentiation of ADSCs partly via activation of the PI3K/Akt signaling pathway. *J Orthop Surg Res* 17, 107.

Lu, C., Miclau, T., Hu, D., Hansen, E., Tsui, K., Puttlitz, C., Marcucio, R.S., 2005. Cellular basis for age-related changes in fracture repair. *J Orthop Res*.

Lu, J., Chatterjee, M., Schmid, H., Beck, S., Gawaz, M., 2016. CXCL14 as an emerging immune and inflammatory modulator. *J Inflamm (Lond)* 13, 1.

Lucas, A.M., Stettenheim, P.R., 1972. *Avian Anatomy: Integument*. United States Department of Agriculture, Washington, D.C.

Lwigale, P.Y., Schneider, R.A., 2008. Other chimeras: quail-duck and mouse-chick. *Methods in cell biology* 87, 59-74.

Mandegar, M.A., Huebsch, N., Frolov, E.B., Shin, E., Truong, A., Olvera, M.P., Chan, A.H., Miyaoka, Y., Holmes, K., Spencer, C.I., Judge, L.M., Gordon, D.E., Eskildsen, T.V., Villalta, J.E., Horlbeck, M.A., Gilbert, L.A., Krogan, N.J., Sheikh, S.P., Weissman, J.S.,

Qi, L.S., So, P.L., Conklin, B.R., 2016. CRISPR Interference Efficiently Induces Specific and Reversible Gene Silencing in Human iPSCs. *Cell Stem Cell* 18, 541-553.

McGrath, K.E., Koniski, A.D., Maltby, K.M., McGann, J.K., Palis, J., 1999. Embryonic expression and function of the chemokine SDF-1 and its receptor, CXCR4. *Dev Biol* 213, 442-456.

Merrill, A.E., Eames, B.F., Weston, S.J., Heath, T., Schneider, R.A., 2008. Mesenchyme-dependent BMP signaling directs the timing of mandibular osteogenesis. *Development* 135, 1223-1234.

Meuter, S., Schaerli, P., Roos, R.S., Brandau, O., Bosl, M.R., von Andrian, U.H., Moser, B., 2007. Murine CXCL14 is dispensable for dendritic cell function and localization within peripheral tissues. *Mol Cell Biol* 27, 983-992.

Mitgutsch, C., Wimmer, C., Sanchez-Villagra, M.R., Hahnloser, R., Schneider, R.A., 2011. Timing of ossification in duck, quail, and zebra finch: intraspecific variation, heterochronies, and life history evolution. *Zoological Science* 28, 491-500.

Miyamoto, S., Takaoka, K., 1993. Bone induction and bone repair by composites of bone morphogenetic protein and biodegradable synthetic polymers. *Ann Chir Gynaecol Suppl* 207, 69-75.

Myers, T.J., Longobardi, L., Willcockson, H., Temple, J.D., Tagliafierro, L., Ye, P., Li, T., Esposito, A., Moats-Staats, B.M., Spagnoli, A., 2015. BMP2 Regulation of CXCL12 Cellular, Temporal, and Spatial Expression is Essential During Fracture Repair. *J Bone Miner Res* 30, 2014-2027.

Nara, N., Nakayama, Y., Okamoto, S., Tamura, H., Kiyono, M., Muraoka, M., Tanaka, K., Taya, C., Shitara, H., Ishii, R., Yonekawa, H., Minokoshi, Y., Hara, T., 2007. Disruption of CXC motif chemokine ligand-14 in mice ameliorates obesity-induced insulin resistance. *J Biol Chem* 282, 30794-30803.

Nassari, S., Duprez, D., Fournier-Thibault, C., 2017. Non-myogenic Contribution to Muscle Development and Homeostasis: The Role of Connective Tissues. *Front Cell Dev Biol* 5, 22.

Noden, D.M., 1978. The control of avian cephalic neural crest cytodifferentiation. I. Skeletal and connective tissues. *Develop Biol* 67, 296-312.

Noden, D.M., Schneider, R.A., 2006. Neural crest cells and the community of plan for craniofacial development: historical debates and current perspectives. *Adv Exp Med Biol* 589, 1-23.

Ojeda, A.F., Munjaal, R.P., Lwigale, P.Y., 2013. Expression of CXCL12 and CXCL14 during eye development in chick and mouse. *Gene Expr Patterns* 13, 303-310.

Oka, K., Oka, S., Sasaki, T., Ito, Y., Bringas, P., Jr., Nonaka, K., Chai, Y., 2007. The role of TGF-beta signaling in regulating chondrogenesis and osteogenesis during mandibular development. *Dev Biol* 303, 391-404.

Park, B.-Y., Hong, C.-S., Sohail, F.A., Saint-Jeannet, J.-P., 2009. Developmental expression and regulation of the chemokine CXCL14 in *Xenopus*. *The International journal of developmental biology* 53, 535-540.

Parker, S.E., Mai, C.T., Canfield, M.A., Rickard, R., Wang, Y., Meyer, R.E., Anderson, P., Mason, C.A., Collins, J.S., Kirby, R.S., Correa, A., 2010. Updated National Birth Prevalence estimates for selected birth defects in the United States, 2004-2006. Birth defects research. Part A, Clinical and molecular teratology 88, 1008-1016.

Phelps, A.M., 1891. Transplantation of Tissue from Lower Animals to Man: Abstract of the Case of Bone-Transplantation at Charity Hospital, Blackwell's Island, N. Y. Daniels Tex Med J 6, 373-384.

Presnell, J., Schreibman, M., Humason, G., 1997. Humason's animal tissue techniques. Johns Hopkins University Press, Baltimore, MD, p. 572.

Proudfoot, A.E., 2002. Chemokine receptors: multifaceted therapeutic targets. Nat Rev Immunol 2, 106-115.

Qi, L.S., Larson, M.H., Gilbert, L.A., Doudna, J.A., Weissman, J.S., Arkin, A.P., Lim, W.A., 2013. Repurposing CRISPR as an RNA-guided platform for sequence-specific control of gene expression. Cell 152, 1173-1183.

Rális, Z.A., Rális, H.M., 1975. A simple method for demonstration of osteoid in paraffin sections. Med Lab Technol 32, 203-213.

Reddi, A.H., Cunningham, N.S., 1993. Initiation and promotion of bone differentiation by bone morphogenetic proteins. J Bone Miner Res 8 Suppl 2, S499-502.

Reinhard, J., Roll, L., Faissner, A., 2017. Tenascins in Retinal and Optic Nerve Neurodegeneration. Front Integr Neurosci 11, 30.

Ricklefs, R.E., Starck, J.M., 1998. Embryonic Growth and Development, in: Starck, J.M., Ricklefs, R.E. (Eds.), Avian growth and development : evolution within the altricial-precocial spectrum. Oxford University Press, New York, pp. 31-58.

Robledo, R.F., Rajan, L., Li, X., Lufkin, T., 2002. The Dlx5 and Dlx6 homeobox genes are essential for craniofacial, axial, and appendicular skeletal development. *Genes Dev* 16, 1089-1101.

Sakabe, T., Sakai, K., Maeda, T., Sunaga, A., Furuta, N., Schweitzer, R., Sasaki, T., Sakai, T., 2018. Transcription factor scleraxis vitally contributes to progenitor lineage direction in wound healing of adult tendon in mice. *J Biol Chem* 293, 5766-5780.

Samee, N., Geoffroy, V., Marty, C., Schiltz, C., Vieux-Rochas, M., Levi, G., de Vernejoul, M.C., 2008. Dlx5, a positive regulator of osteoblastogenesis, is essential for osteoblast-osteoclast coupling. *Am J Pathol* 173, 773-780.

Sato, N., Meijer, L., Skaltsounis, L., Greengard, P., Brivanlou, A.H., 2004. Maintenance of pluripotency in human and mouse embryonic stem cells through activation of Wnt signaling by a pharmacological GSK-3-specific inhibitor. *Nat Med* 10, 55-63.

Satokata, I., Maas, R., 1994. *Msx1* deficient mice exhibit cleft palate and abnormalities of craniofacial and tooth development. *Nat Genet* 6, 348-356.

Schindelin, J., Arganda-Carreras, I., Frise, E., Kaynig, V., Longair, M., Pietzsch, T., Preibisch, S., Rueden, C., Saalfeld, S., Schmid, B., Tinevez, J.Y., White, D.J., Hartenstein, V., Eliceiri, K., Tomancak, P., Cardona, A., 2012. Fiji: an open-source platform for biological-image analysis. *Nat Methods* 9, 676-682.

Schneider, R.A., 1999. Neural crest can form cartilages normally derived from mesoderm during development of the avian head skeleton. *Develop Biol* 208, 441-455.

Schneider, R.A., 2005. Developmental mechanisms facilitating the evolution of bills and quills. *J Anat* 207, 563-573.

Schneider, R.A., 2015. Regulation of Jaw Length During Development, Disease, and Evolution. *Curr Top Dev Biol* 115, 271-298.

Schneider, R.A., Eames, B.F., 2004. Neural Crest Mesenchyme Regulates the Timing of Intramembranous Ossification. 50th Annual Meeting of the Orthopaedic Research Society, San Francisco, CA.

Schneider, R.A., Helms, J.A., 2003. The cellular and molecular origins of beak morphology. *Science* 299, 565-568.

Schneider, R.A., Hu, D., Helms, J.A., 1999. From head to toe: conservation of molecular signals regulating limb and craniofacial morphogenesis. *Cell and Tissue Research* 296, 103-109.

Schneider, R.A., Hu, D., Rubenstein, J.L., Maden, M., Helms, J.A., 2001. Local retinoid signaling coordinates forebrain and facial morphogenesis by maintaining FGF8 and SHH. *Development* 128, 2755-2767.

Sharpe, P.M., Ferguson, M.W., 1988. Mesenchymal influences on epithelial differentiation in developing systems. *Journal of Cell Science. Supplement* 10, 195-230.

Smith, F.J., Percival, C.J., Young, N.M., Hu, D., Schneider, R.A., Marcucio, R.S., Hallgrimsson, B., 2015. Divergence of craniofacial developmental trajectories among avian embryos. *Dev Dyn*.

Smith, S.S., Chu, D., Qu, T., Aggleton, J.A., Schneider, R.A., 2022. Species-specific sensitivity to TGFbeta signaling and changes to the Mmp13 promoter underlie avian jaw development and evolution. *Elife* 11.

Smith, S.S., Dole, N.S., Franceschetti, T., Hrdlicka, H.C., Delany, A.M., 2016. MicroRNA-433 Dampens Glucocorticoid Receptor Signaling, Impacting Circadian Rhythm and Osteoblastic Gene Expression. *J Biol Chem* 291, 21717-21728.

Solem, R.C., Eames, B.F., Tokita, M., Schneider, R.A., 2011. Mesenchymal and mechanical mechanisms of secondary cartilage induction. *Dev Biol* 356, 28-39.

Song, X., Wang, S., Li, L., 2014. New insights into the regulation of Axin function in canonical Wnt signaling pathway. *Protein Cell* 5, 186-193.

Starck, J.M., Ricklefs, R.E., 1998. Avian growth and development: evolution within the altricial-precocial spectrum. Oxford University Press on Demand.

Stein, G.S., Lian, J.B., van Wijnen, A.J., Stein, J.L., Montecino, M., Javed, A., Zaidi, S.K., Young, D.W., Choi, J.Y., Pockwinse, S.M., 2004. Runx2 control of organization, assembly and activity of the regulatory machinery for skeletal gene expression. *Oncogene* 23, 4315-4329.

Sun, S., Yu, M., Fan, Z., Yeh, I.T., Feng, H., Liu, H., Han, D., 2019. DLX3 regulates osteogenic differentiation of bone marrow mesenchymal stem cells via Wnt/beta-catenin pathway mediated histone methylation of DKK4. *Biochem Biophys Res Commun* 516, 171-176.

Tachibana, K., Hirota, S., Iizasa, H., Yoshida, H., Kawabata, K., Kataoka, Y., Kitamura, Y., Matsushima, K., Yoshida, N., Nishikawa, S., Kishimoto, T., Nagasawa, T., 1998. The chemokine receptor CXCR4 is essential for vascularization of the gastrointestinal tract. *Nature* 393, 591-594.

Takeuchi, J.K., Koshiba-Takeuchi, K., Suzuki, T., Kamimura, M., Ogura, K., Ogura, T., 2003. Tbx5 and Tbx4 trigger limb initiation through activation of the Wnt/Fgf signaling cascade. *Development* 130, 2729-2739.

Tokita, M., Schneider, R.A., 2009. Developmental origins of species-specific muscle pattern. *Dev Biol* 331, 311-325.

Toriumi, D.M., Kotler, H.S., Luxenberg, D.P., Holtrop, M.E., Wang, E.A., 1991. Mandibular reconstruction with a recombinant bone-inducing factor. Functional, histologic, and biomechanical evaluation. *Arch Otolaryngol Head Neck Surg* 117, 1101-1112.

Trainor, P.A., Dixon, J., Dixon, M.J., 2009. Treacher Collins syndrome: etiology, pathogenesis and prevention. *Eur J Hum Genet* 17, 275-283.

Tran, D.L., Imura, H., Mori, A., Suzuki, S., Niimi, T., Ono, M., Sakuma, C., Nakahara, S., Nguyen, T.T.H., Pham, P.T., Hoang, V., Tran, V.T.T., Nguyen, M.D., Natsume, N., 2018.

Association of MEOX2 polymorphism with nonsyndromic cleft palate only in a Vietnamese population. *Congenit Anom (Kyoto)* 58, 124-129.

Tyler, M.S., Hall, B.K., 1977. Epithelial influences on skeletogenesis in the mandible of the embryonic chick. *Anatomical Record* 188.

Tyler, M.S., McCobb, D.P., 1980. The genesis of membrane bone in the embryonic chick maxilla: epithelial-mesenchymal tissue recombination studies. *Journal of Embryology and Experimental Morphology* 56, 269-281.

Urist, M.R., 1965. Bone: formation by autoinduction. *Science* 150, 893-899.

Vaglia, J.L., Hall, B.K., 1999. Regulation of neural crest cell populations: occurrence, distribution and underlying mechanisms. *International Journal of Developmental Biology* 43, 95-110.

Van Exan, R.J., Hall, B.K., 1984. Epithelial induction of osteogenesis in embryonic chick mandibular mesenchyme studied by transfilter tissue recombinations. *Journal of Embryology and Experimental Morphology* 79, 225-242.

Varadi, M., Anyango, S., Deshpande, M., Nair, S., Natassia, C., Yordanova, G., Yuan, D., Stroe, O., Wood, G., Laydon, A., Zidek, A., Green, T., Tunyasuvunakool, K., Petersen, S., Jumper, J., Clancy, E., Green, R., Vora, A., Lutfi, M., Figurnov, M., Cowie, A., Hobbs, N., Kohli, P., Kleywegt, G., Birney, E., Hassabis, D., Velankar, S., 2022. AlphaFold Protein Structure Database: massively expanding the structural coverage of protein-sequence space with high-accuracy models. *Nucleic Acids Res* 50, D439-D444.

Vlashi, R., Zhang, X., Wu, M., Chen, G., 2023. Wnt signaling: Essential roles in osteoblast differentiation, bone metabolism and therapeutic implications for bone and skeletal disorders. *Genes Dis* 10, 1291-1317.

Wang, E.A., Rosen, V., D'Alessandro, J.S., Bauduy, M., Cordes, P., Harada, T., Israel, D.I., Hewick, R.M., Kerns, K.M., LaPan, P., et al., 1990. Recombinant human bone morphogenetic protein induces bone formation. *Proc Natl Acad Sci U S A* 87, 2220-2224.

Wang, H., He, X.Q., Jin, T., Li, Y., Fan, X.Y., Wang, Y., Xu, Y.Q., 2016. Wnt11 plays an important role in the osteogenesis of human mesenchymal stem cells in a PHA/FN/ALG composite scaffold: possible treatment for infected bone defect. *Stem Cell Res Ther* 7, 18.

Wang, N., Butler, J.P., Ingber, D.E., 1993. Mechanotransduction across the cell surface and through the cytoskeleton. *Science* 260, 1124-1127.

Wang, X.P., O'Connell, D.J., Lund, J.J., Saadi, I., Kuraguchi, M., Turbe-Doan, A., Cavallesco, R., Kim, H., Park, P.J., Harada, H., Kucherlapati, R., Maas, R.L., 2009. Apc inhibition of Wnt signaling regulates supernumerary tooth formation during embryogenesis and throughout adulthood. *Development* 136, 1939-1949.

Wedden, S.E., 1987. Epithelial-mesenchymal interactions in the development of chick facial primordia and the target of retinoid action. *Development* 99, 341-351.

Westrich, J.A., Vermeer, D.W., Colbert, P.L., Spanos, W.C., Pyeon, D., 2020. The multifarious roles of the chemokine CXCL14 in cancer progression and immune responses. *Mol Carcinog* 59, 794-806.

Williams, R.M., Senanayake, U., Artibani, M., Taylor, G., Wells, D., Ahmed, A.A., Sauka-Spengler, T., 2018. Genome and epigenome engineering CRISPR toolkit for in vivo modulation of cis-regulatory interactions and gene expression in the chicken embryo. *Development* 145.

Wodarz, A., Nusse, R., 1998. Mechanisms of Wnt signaling in development. *Annu Rev Cell Dev Biol* 14, 59-88.

Woronowicz, K.C., Gline, S.E., Herfat, S.T., Fields, A.J., Schneider, R.A., 2018. FGF and TGFbeta signaling link form and function during jaw development and evolution. *Dev Biol* 444 Suppl 1, S219-S236.

Wozney, J.M., Rosen, V., Celeste, A.J., Mitsock, L.M., Whitters, M.J., Kriz, R.W., Hewick, R.M., Wang, E.A., 1988. Novel Regulators of Bone Formation: Molecular Clones and Activities. *Science* 242, 1528-1534.

Wu, L.Z., Xu, X.Y., Liu, Y.F., Ge, X., Wang, X.J., 2015. Expansion of polyalanine tracts in the QA domain may play a critical role in the clavicular development of cleidocranial dysplasia. *J Genet* 94, 551-553.

Wu, X., Wang, X., Shan, L., Zhou, J., Zhang, X., Zhu, E., Yuan, H., Wang, B., 2021. High-mobility group AT-Hook 1 mediates the role of nuclear factor I/X in osteogenic differentiation through activating canonical Wnt signaling. *Stem Cells* 39, 1349-1361.

Yan, Y., Tang, D., Chen, M., Huang, J., Xie, R., Jonason, J.H., Tan, X., Hou, W., Reynolds, D., Hsu, W., Harris, S.E., Puzas, J.E., Awad, H., O'Keefe, R.J., Boyce, B.F.,

Chen, D., 2009. Axin2 controls bone remodeling through the beta-catenin-BMP signaling pathway in adult mice. *J Cell Sci* 122, 3566-3578.

Yeo, N.C., Chavez, A., Lance-Byrne, A., Chan, Y., Menn, D., Milanova, D., Kuo, C.C., Guo, X., Sharma, S., Tung, A., Cecchi, R.J., Tuttle, M., Pradhan, S., Lim, E.T., Davidsohn, N., Ebrahimkhani, M.R., Collins, J.J., Lewis, N.E., Kiani, S., Church, G.M., 2018. An enhanced CRISPR repressor for targeted mammalian gene regulation. *Nat Methods* 15, 611-616.

Yu, H.M., Jerchow, B., Sheu, T.J., Liu, B., Costantini, F., Puzas, J.E., Birchmeier, W., Hsu, W., 2005. The role of Axin2 in calvarial morphogenesis and craniosynostosis. *Development* 132, 1995-2005.

Zernik, J., Twarog, K., Upholt, W.B., 1990. Regulation of alkaline phosphatase and alpha 2(I) procollagen synthesis during early intramembranous bone formation in the rat mandible. *Differentiation* 44, 207-215.

Zhang, J., Zhang, W., Dai, J., Wang, X., Shen, S.G., 2019. Overexpression of Dlx2 enhances osteogenic differentiation of BMSCs and MC3T3-E1 cells via direct upregulation of Osteocalcin and Alp. *Int J Oral Sci* 11, 12.

Zou, Y.R., Kottmann, A.H., Kuroda, M., Taniuchi, I., Littman, D.R., 1998. Function of the chemokine receptor CXCR4 in haematopoiesis and in cerebellar development. *Nature* 393, 595-599.

Publishing Agreement

It is the policy of the University to encourage open access and broad distribution of all theses, dissertations, and manuscripts. The Graduate Division will facilitate the distribution of UCSF theses, dissertations, and manuscripts to the UCSF Library for open access and distribution. UCSF will make such theses, dissertations, and manuscripts accessible to the public and will take reasonable steps to preserve these works in perpetuity.

I hereby grant the non-exclusive, perpetual right to The Regents of the University of California to reproduce, publicly display, distribute, preserve, and publish copies of my thesis, dissertation, or manuscript in any form or media, now existing or later derived, including access online for teaching, research, and public service purposes.

DocuSigned by:

An Nhat Duy Nguyen

AFA19A84CF93497...

Author Signature

8/28/2023

Date